Influence of Astrocytes on Working Memory

Valentin Würzbauer

Master of Science Thesis

TU Delft Delft University of Technology

Delft Center for Systems and Control

Influence of Astrocytes on Working Memory

Master of Science Thesis

For the degree of Master of Science in Systems and Control at Delft University of Technology

Valentin Würzbauer

May 15, 2023

Faculty of Mechanical, Maritime and Materials Engineering (3mE) · Delft University of Technology

Abstract

The central nervous system is the key controller in the human body. All aspects of live - from basic functions such as breathing to higher cognitive processes as memory building or complex decision making - have a network of neural cells at its core. While neuronal cells have been subject to intensive research for more than a century, the role of glial cells - the second major group of cell types in the brain - including astrocytes is still relatively unknown or contradictory. The focus of this thesis lies on memory processes and the astrocytic impact on them.

Working memory is a memory module which describes the short-term storage and processing of input data. A classic example is remembering a phone number before noting it down or typing it. Working memory is the fundamental building block for many cognitive functions such as prediction, goal-directed behavior and decision-making. Its impairment is tragically visible in various forms of dementia which can be caused by Alzheimer's Disease or Parkinson's Disease. Understanding the role of an astrocytic pathway as a possible underlying mechanism of working memory, could help strategies to prevent and treat these diseases and improve patients' quality of life.

The goal of this thesis is to provide support for astrocytic gliotransmission as a fundamental pathway in regard to Working memory. To this end, stability analysis of a tripartite model with novel modifications shows the ability of extended firing in the presence of gliotransmission and hence, the principal ability for memory storage. Building upon this cell model, a complex network consisting of an established neuron-astrocyte structure is investigated. Different simulation scenarios show the possibility of astrocytes to store neuronal information during the absence of input signal and thus, showing a possible method for working memory. Simultaneously, two competing theories of persistent and sparse delay activity are explained by varying strength of astrocytic gliotransmission while showing working memory functionality for both cases. Classical working memory experiments on primates are used as guiding points for the simulation sequence in order to provide comparability and authenticity.

Table of Contents

List of Figures

List of Tables

Acknowledgements

I would like to thank my supervisor Dr. Matin Jafarian from TU Delft and my co-supervisor Dr. Kerstin Lenk from TU Graz for their great support during my master thesis. The completion of my thesis project would have surely not been possible without their help. The long distance has not prevented constructive discussions and good communication and I feel strong gratitude towards them.

Delft, University of Technology
May 15, 2023

Valentin Würzbauer

Chapter 1

Introduction

Understanding the human brain is a key scientific challenge that is tackled by numerous researchers as far back as the times of the neuroscientific pioneers Cajal and Golgi in the late nineteenth and early twentieth century. Our central nervous system (CNS) controls every step that we take and every decision that we make. It is unparalleled in its importance. The sheer size and complexity of this biological network that builds up the human nervous system makes it a demanding and long-lasting field or research. Learning and retrieving memories are vital for our survival and essential processes of the CNS. Working memory (WM) forms a fundamental component of planning and decision-making and is basically active at any moment in our life.

1-1 Motivation

The incentives for research in the field of biological neural networks are versatile but two main roots stand out - the treatment of neurological disorders and the investigation of artificial intelligence. While the role of neurons within the nervous system has been deeply investigated, the interest for astrocytes - a type of glial cells commonly found in the central nervous system - regarding its involvement in signal transmission has drawn attention only in the recent decades and thus a large amount of research is still to be done.

A large number of common diseases such as Alzheimer's Disease, Parkinson's Disease, epilepsy or bipolar disorder are caused by a malfunctioning nervous system and understanding the processes involved can be crucial in prevention and treatment strategies. In the context of memory deficits, dementia is probably the first symptom that comes to mind affecting millions of people world wide [6]. Being caused by several diseases including Alzheimer's Disease [7], vascular dementia, Parkinson's Disease [8] and frontotemporal dementia, dementia is characterized by significant loss of memory function in combination with an additional cognitive deficit and causes immense limitation in quality of life.

Further motivation is given by the fact that modern technology relies heavily on research results of the central nervous system. The term neural networks is currently mostly associated with artificial neural networks (ANNs) for various machine learning purposes ranging from smart selection of personalized advertisement [9] to automated decision-making in autonomous vehicles [10]. The main idea behind ANN is the observation that synaptic connections in the biological nervous system act as adaptive parameter in order to learn and include new experiences. Biologically inspired mathematical models which are trained and optimized for specific tasks are applied in numerous modern developments. While traditional ANNs have only considered neurons as elements of their networks, there is a promising attempt in [11] that has presented performance improvement for classification problems when artificial astrocytes where included in ANN creating the first artificial neuron-glial networks (NGN). It should be mentioned that while original ANNs use concepts that resemble biological neural networks, current developments that have optimized machine learning performance have introduced significant differences to their biological counterparts in order to improve training processes [9]. On the other side, the idea of changing synaptic weights in order to remember certain input-output relations is a common fundamental element in both biological as well as artificial neuronal networks and strongly relates to the field of memory processes.

The perspective taken in this thesis focuses on fundamental ways of storing information in the memory while considering the biological processes in an appropriate but surely simplified way. The field of computational neuroscience uses mathematical models of the human brain or parts of it in order to conduct research on the topics mentioned above. In principle, the nervous system may be considered a large-scale electrical network or circuit with various nonlinear elements including neurons and astrocytes as its most important components.

1-2 Background - Memory and Astrocytes

In the following, basic concepts and scientific models of memory with varying biological accuracy are introduced. Additionally, necessary background of biology regarding the human nervous system is brought up in order to connect the abstract idea of memory with its concrete biological counterpart.

1-2-1 Basics of Memory

"Learning and memory are two of the most magical capabilities of our mind. Learning is the biological process of acquiring new knowledge about the world, and memory is the process of retaining and reconstructing that knowledge over time [12]." Memory is the foundation of reasoning, decision-making and in principal all of our behavior. It is therefore crucial for our survival and understanding the underlying mechanisms could provide enormous progress in medical fields. Since the topic itself gives content for an immense amount of literature, only a short pathway is drawn from the fundamental understanding of storing information to the relation of memory to neuron-astrocyte network models.

Several abstract models regarding memory have been developed over the years in order to tackle the overall complexity of this area and enable a systematic research approach. The

memory model by Atkinson and Shiffrin [1] is probably the most influential one. While the model is not based on biological processes, it gives a meaningful concept that is supported by their experiments. The model consists of two parts, a rigorous memory structure and flexible control processes that connect it. The memory structure itself is build up by the sensory register, the short-term store and the long-term store. The fragmentation of memory or the differentiation in short and long term memory has been under strong debate but is supported by various patients that have suffered lesions only affecting short but not long-term memory [1]. The main idea is that external sensory signals from various sources are passing each memory blocks in series and depending on the significance of the information compared to the current priorities it passes on or it is dismissed. Control processes on the other hand

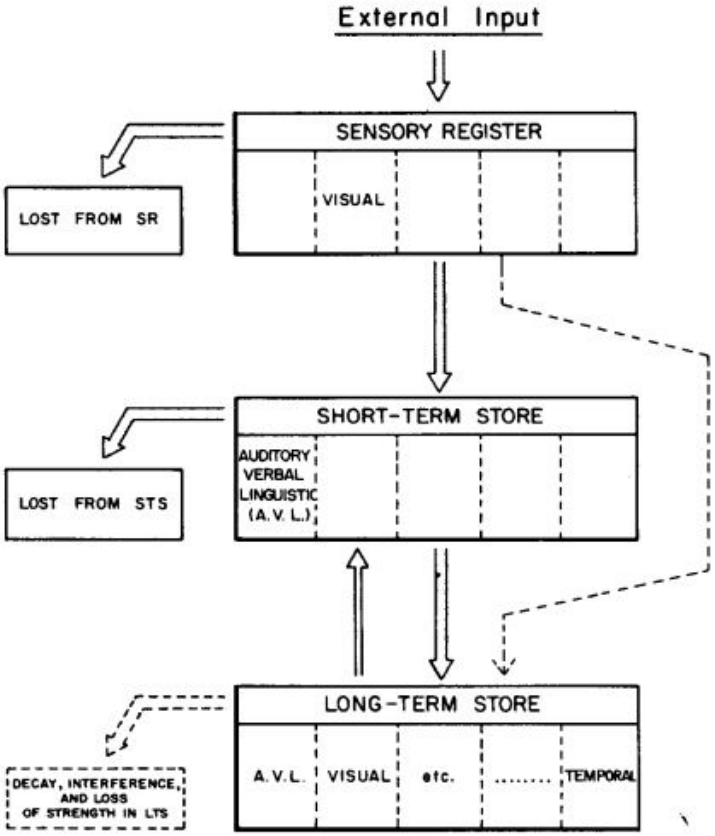

FIG. 1. Structure of the memory system.

Figure 1-1: Structure of Memory Model by Atkinson & Shiffrin [1]: An external input is registered in the Sensory Register at the time-scale over hundreds of milliseconds. In case, the transition into the Short-Term Store is successfully conducted, the information can be stored for up to 15 to 30 seconds. In the Long-Term Store information are saved without any decay and potentially stays there for the whole life. Interaction between the stores are defined by Control Processes.

describe "nonpermanent features of memory" [1] and are under control of the memory holder. Examples for this are priority of attention and type of rehearsing patterns for the sensory register, search and retrieval processes in the short-term storage and the transfer between short-term and long-term storage. In Figure 1-1, the classic pathway within this multi-store

memory model runs from the sensory register via the short-term store into the long-term store with processes controlling this transitions.

In [13], a pioneering model for working memory has been introduced by Baddeley. The results of psychological experiments on students regarding reasoning, comprehension and free recall has lead to the theory of WM consisting of "storage and control processing" of information within a distinctive time limit. The model by [13] consists of four elements being the central executive and its subcomponents - the phonological loop, the episodic buffer and the visuospatial sketchpad. The idea is that the central executives act as a supervisory instrument for the three sensory dependent agents corresponding to audio, event and visual inputs.

WM has mainly been linked to the prefrontal cortex (PFC) in the human brain. Electrophysiological experiments on primates and rodents have shown activity in the prefrontal cortex during working memory tasks such as delayed-response exercises with visual stimuli. An important discovery is that specific groups of neurons in the PFC are stimulated by specific inputs leading to so called memory fields or receptive fields which can provide a way of encoding and possibly storing a specific input signal. The prefrontal cortex consists mostly of excitatory pyramidal neurons and inhibitory interneurons forming complex circuits [14], [15].

The manner of how information is stored in the brain for a long-term has been under strong debate in the nineteenth and twentieth century but nowadays the theory that memory is encoded in synaptic strength dominates. An alternative theory says that specific neurons correspond to specific data pieces which are also referred to as "grandmother cells" [16].

1-2-2 Biological Fundamentals of the Nervous System

The human nervous system consists of an extremely large and complex network of neural cells. It reaches through the entire body and can be distinguished into the central (CNS) and the peripheral nervous system (PNS). While the central nervous system consists of the spinal cord and the brain and is considered the main control organ of the body, the peripheral nervous system is build up by widely spread neurons whose task is to sense input from the environment and send this information to the CNS as well as transmit control signals from the CNS to actuators such as muscles. Tasks of the CNS include information processing, motion control and higher cognitive functions such as prediction, planning and decision-making [17].

The two main cell types building up the CNS are neurons and glial cells. Neurons or nerve cells is a highly specialized cell class that uses electrochemical signalling to transmit and process information. Glial cells on the other side form a less uniform cell class compared to the neurons. The four major glial cell types are Schwann cells and oligodentrocytes, micro glia, neuron-glia 2 cells and astrocytes. They perform various tasks in order to support the structure, energy supply, signal transmission or defense response for the neuronal network. In contrast to the neurons, the significance of glial cells has only become apparent in the second half of the twentieth century and therefore this research area is still rather open [2].

Neurons

A neuron can be described by its core elements being dendrites, the soma and the axon. Figure 1-2 shows a simplified graphic of this structure. The aboreal dendrites connect the neuron to other neurons and act as receiver of both excitatory and inhibitory electrical and electrochemical signals in form of ions or neurotransmitter. The sum of incoming charges is transmitted to the axon hillock where it is processed and in case of exceeding a voltage threshold an action potential is send through the axon. The axon connects the neuron to other neurons and works as a sender. Myelin sheath - created by oligodentrocytes in the CNS and Schwann cells in the PNS - wraps around the axon in order to reduce the voltage leakage.

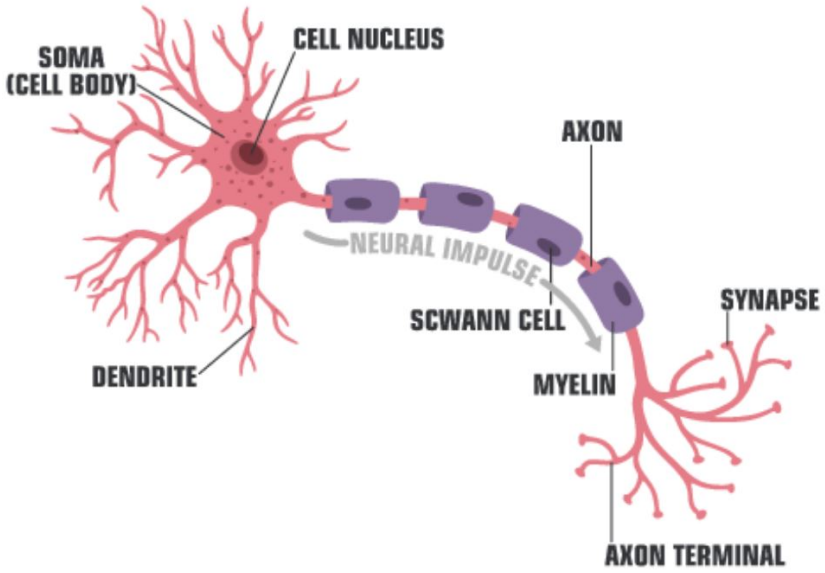

Figure 1-2: Structure of a Standard Neuron: A classical neuron is portrayed consisting of the main components - the soma, the dendrites and the axon. Additionally, a glial cell - the oligodendrocyte - is shown enwrapping the axon.

The key components for the generation of action potentials are voltage dependent ion channels in the cell membrane of neurons. The cell membrane separates the cytoplasm and extracellular fluid which both contain specific concentrations of ions - most importantly sodium, potassium, calcium and chloride. Ion selective channels, ion pumps and ion specific cell membrane permeability lead to different ion concentration inside and outside the cell membrane. The Nernst equation reflects the different mechanism which leads to an electrical and chemical balance. As a result, the neural cytoplasm is charged at around $-70mV$ in humans. This resting potential differs from neuron to neuron depending on the exact composition of the cell membrane w.r.t. ion channels and ion pumps [18].

The sequence of an action potential (AP) can be illustrated using Figure 1-3. Phase **0-1** describes the resting states at around $-70mV$. Incoming electrical signals bring the voltage up to a threshold value which leads to opening of voltage gated sodium channel (VGSC) and a positive sodium ion flow from the extracellular space into the cytoplasm between **1-2**. Consequently, the cytoplasm depolarizes significantly in a very short time. At **2**, the VGSCs are

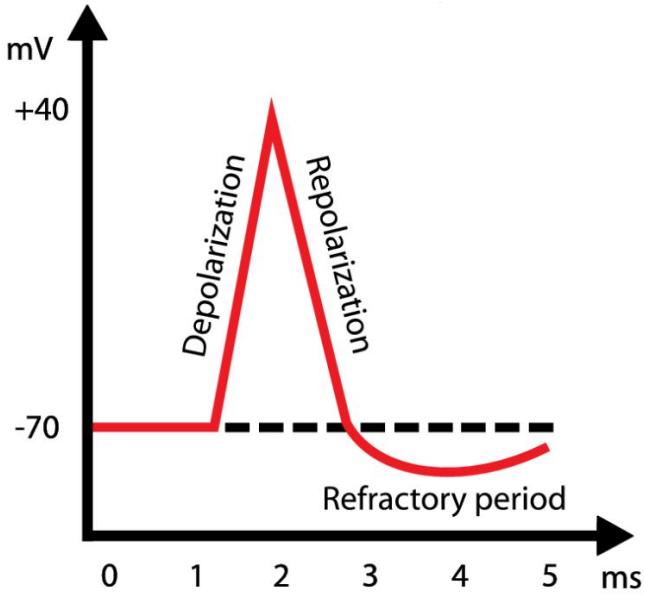

Figure 1-3: Schematic Course of an Action Potential

inactivated due to the high positive membrane potential and instead voltage gated potassium channels (VGPC) are opened allowing positive potassium to leave the neuron and resulting into hyperpolarization of the neuron. After inactivation of the VGPCs at **3**, ion pumps and membrane permeability slowly restore the formerly existing resting state **5** with resting potential. The phase between **3** and **5** is called refractory period and another action potential can not be generated during that phase. It is important to mention that the evolution of an AP occurs within the time interval of a few milliseconds. [17].

Astrocytes

The term neuroglia has been introduced by Rudolph Virchow in 1856 in order to describe the matter in between the neurons or *Zwischenmasse* (in-between mass). Astrocytes have been named after their star-like shape w.r.t. to the greek astéri [19]. Astrocytes or Astroglia classify neural cells which show large variety regarding shape and function linked to the nervous system. Their tasks include the energy supply and protection of neurons as well as regulation of extracellular ions and neurotransmitter. In order to fulfill this functions, astrocytes are generally connected to multiple blood vessels, neurons and even neighbouring astrocytes [19].

An astrocyte in the hippocampus has a soma diameter of ca. 7-9 micrometer and can connect with approximately 140.000 synapses which are in average from round 8 neurons [2]. Figure 1-4 gives an impression of the arboreal cell structure. The left image of Figure 1-4 shows blue-coloured neurons in the background and two distinct astrocytes in green and red. In the right image, a neuron can be seen in red and an astrocyte next to it in green. The pictures display the delicate and complex structures of astrocytes even compared to neurons. An important difference to neurons, is the non-excitability of astrocytes. As a consequence, classical experiments on neurons using electrodes provide little information for astrocytes regarding

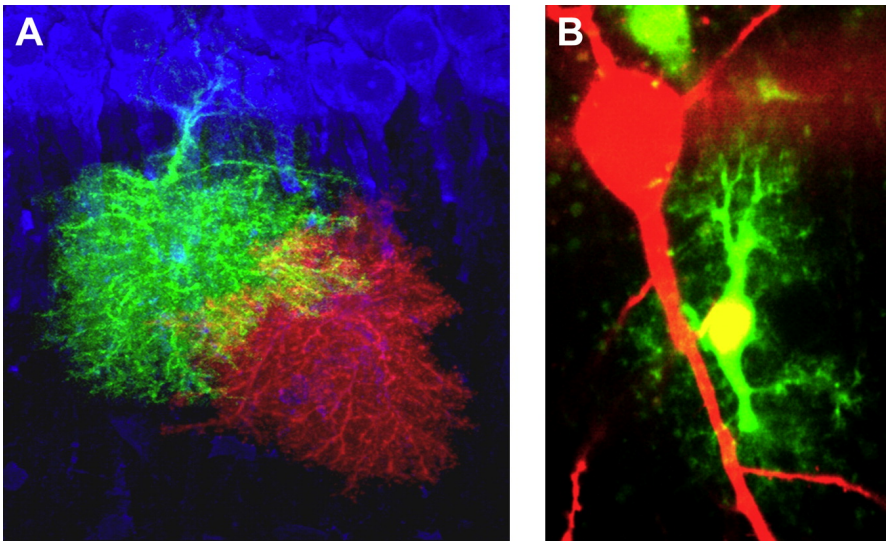

Figure 1-4: Pictures of Astrocytes via Ca^{2+} Indicator Dyes [2]. Picture A: Two astrocytes are depicted in the colors green and red while neurons are dyed blue. Picture B: Red neuron and green astrocyte

their role in communication which is one of the reason why the research on astrocytes started much later than neurons. Instead calcium oscillations are the dominant signalling forms of astrocytes [20].

Similarly to neurons, astrocytes are connected with each other and the corresponding network is often referred to as syncytium. The links between astrocytes are formed by proteins building gap junctions or connexins. Intercellular calcium oscillations are induced into connected astrocytes via two pathways. Firstly, the connexins allow both calcium ions and as well as the messenger substance inositol 1,4,5-trisphosphate (IP_3) to path through the gap junctions according to the concentration difference. Experiments have shown that passage of IP_3 is the dominant component here [21]. Secondly, astrocytic release of adenosine triphosphate (ATP) - an organic substance that provides cells with energy - into the extracellular space can activate purinergic receptors of neighbouring astrocytes which induces the rise of calcium concentration. It is important to stress that this second mechanism does not depend on any gap junctions and is also less reliable [22].

Interaction of Neurons and Astrocytes

Although other combinations are possible, the most common synaptic connection links a presynaptic axon to a postsynaptic dendrite enabling signal transfer following an AP. The signal transmission can be realized in two different ways - electrically and chemically. The chemical synapse is by far the more common connection type and uses various neurotransmitters [17]. Arriving calcium ions at the end of the presynaptic neuron's axon due to an AP triggers the release of vesicles which contain transmitter molecules. The result is the release of neurotransmitter into the synaptic cleft. Activated by neurotransmitter, ion channels in the postsynaptic dendrites are opening and allowing ions to enter the postsynaptic neuron resulting into either excitatory or inhibitory response depending on the ion type [23]. Addi-

tionally, electrical synapses are found in nervous systems. Bypassing the usage of transmitter molecules, a physical connection between presynaptic and postsynaptic neuron enables a direct ion exchange via gap junctions build by proteins during an AP. A major difference to the chemical synapse is the fact that gap junctions can communicate bidirectionally while neurotransmitter only allow unidirectional signalling. Furthermore, chemical synapses show a small time delay of around 1 ms which is not present for electrical synapses. Electrical synapses play a minor role in the CNS and are therefore omitted in our later model [17].

The idea of a tripartite synapse requires that additionally to the presynaptic and the postsynaptic neuron an astrocyte is added to the synaptic processes [24]. The release of neurotransmitter does not only affect the postsynaptic neuron but also the astrocyte enwrapping the synapse and in return astrocytes respond by releasing gliotransmitter into the synaptic cleft as shown in Figure 1-5.

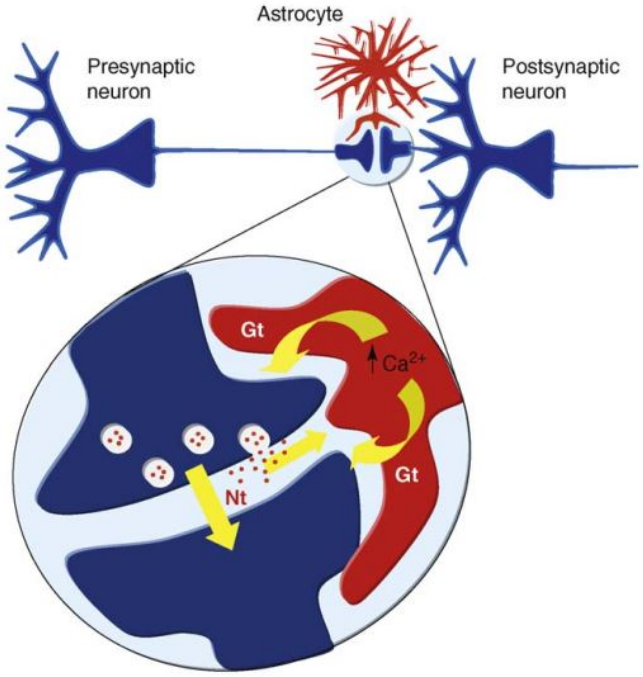

Figure 1-5: Schematic Tripartite Synapse [3]. The release of neurotransmitter (Nt) triggers calcium oscillations (Ca^{2+}) in astrocytes which may lead to the release of gliotransmitter (Gt)

Calcium dynamics of astrocytes which can be affected by neurotransmitter are the foundation of this theory. The main mechanism of calcium elevation in astrocytes is based on calcium ions stored within the endoplasmic reticulum (ER) of the astrocyte which also involves IP_3 as a secondary messenger. There are two ion channels - IP_3R and Ryanodine receptor (RyR) - that are responsible for calcium release from the ER. Calcium elevations usually start with the stimulation of G protein-coupled receptors (GPCRs) at the cell membrane of astrocytes by e.g. neurotransmitters. As a result, "PLC hydrolyzes the membrane lipid phosphatidylinositol 4,5-bisphosphate to generate diacylglycerol (DAG) and IP_3" [2]. The IP_3 activates ion channels at the ER leading to a Ca^{2+} release into the cytoplasm. This process is known as canonical phospholipase C (PLC)/inositol 1,4,5-trisphosphate pathway [2]. The release of

calcium can trigger the activation of further IP_3Rs and RyRs resulting into a calcium induced calcium release process (CICR). The calcium concentration promotes the activation of IP3Rs and RyRs up to a specific threshold and inhibits it for higher concentrations. The result is an oscillatory behavior. As an opposing force, the (sarco)endoplasmic reticulum Ca2+/ATPase (SERCA) pumps are filling the ER with cytosolic calcium ions and regulate/stabilize in that way the oscillations [25].

In response to the calcium oscillations, astrocyte are also able to release transmitter substances - sometimes referred as gliotransmitters - such as glutamate, D-serine, ATP, γ-Aminobutyric acid (GABA), prostaglandins and neuropeptides [26]. The underlying pathways for the release of gliotransmitters are abundant and still poorly understood. Additionally, the existence of gliotransmission in physiological astrocytes is still under debate [27]. Gliotransmission affects both the presynaptic and the postsynpatic neuron. The release probability of neurotransmitter can be altered by the effect on metabotropic glutamate receptors on the presynaptic terminal. At the same time, astrocytic gliotransmitter can induce slow inward current at the postsynaptic terminal by stimulating N-methyl-D-aspartat (NMDA) receptors and thus depolarize the postsynaptic neuron [28].

It is important to mention that the time scale of the astrocytic calcium dynamics is of a different magnitude than the neuronal dynamics. While action potential occur in matter of milliseconds, the calcium oscillations and the connected gliotransmission takes place several seconds after the astrocytic stimulation and has a much longer lasting effect. These characteristics are also the reason why astrocytic gliotransmission is of interest in the field of short-term and working memory.

1-2-3 Theories of Working Memories

The idea of memory being encoded in the strength and dynamics of synaptic connections between neurons has already been postulated by Cajal in 1894 [29] which has later been proven in experiments by [30]. Further on, Hebbian Learning or spike timing dependent plasticity (STDP) has been introduced, theorizing that the synapse between pre- and postsynaptic neuron will only be potentiated if their action potential occurs within a small time period [31]. Hebbian Learning is mostly associated with long-term memory. While short-term synaptic plasticity (STP) is thought to be caused by non-lasting modification such as the effect of the neurotransmitter serotonin, long term synaptic plasticiy (LTP) is linked with the genesis of further receptors in existing synapses commonly via NMDA receptor dependent mechanisms as well as the genesis of new synapses due to gene activation [12]. Experiments have often been conducted on animals with simple nervous systems such as the *Aplysia* and its gill-withdrawal reflex [30] providing evidence for theories on STP and LTP.

The so far mentioned models by [1] and [13] have only been able to give a conceptual grasp of memory processes and have not been shown to rest upon biological experiments or physiological foundation. In the following, experiments and theories are reflected that give more insight in the underlying biological processes that are thought to be linked with memory processes and more specific working memory.

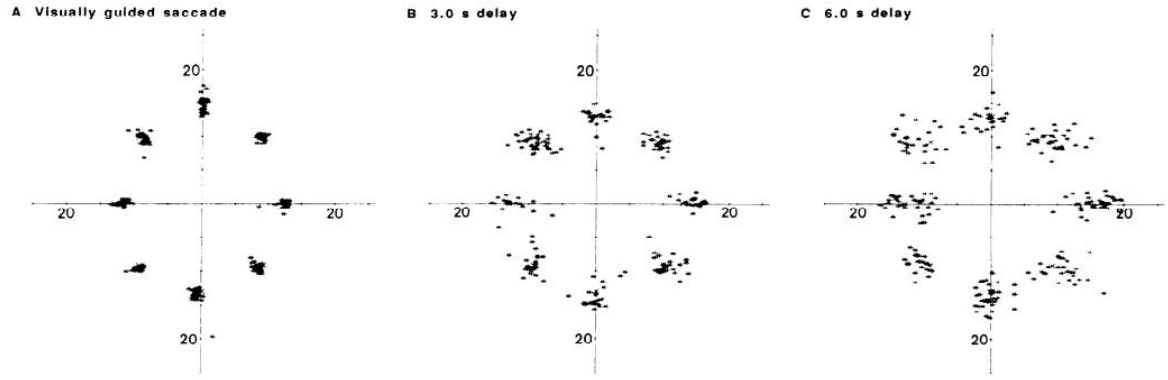

Figure 1-6: Experiment of Oculomotor Delayed Response Task [4]: The experimental results of working memory task for primates is shown. Eight different oculomotor positions are shown to the test subject and recall at 3 seconds and 6 seconds after the stimulation shows fading memory performance.

In order to examine neuronal activity during working memory tasks a number of experiments on rodents and primates have been performed. The general idea of these experiments is to expose the test subject to a specific input and evoke a recall after a specified delay period. One important implementation of this concept has been realized via the oculomotor delayed-response task in [4]. Adult rhesus monkeys have been the subjects of two operations prior to the experiment. Firstly, a search coil has been placed under one eye in order to track eye movement and secondly recording electrodes have been placed inside the prefrontal cortex. The test subjects have been trained to follow a specific test procedure. After a visual stimuli is given to them, a fixation target is shown in the second step. After its disappearance a reward is obtained if the test subjects execute an eye movement in direction to the original visual stimuli. In Figure 1-6, a visualisation of this experiment is shown. Several variations have been conducted using primates or rodents such as mice as test subjects [14]. The results have shown that a specific group of neurons demonstrates sustained activity even during the delay period which stops after the retrieval of the input data and the corresponding reward has been given. This has lead to the persistent activity theory which links the storage of input data in the working memory with the persistent spiking activity of a tuned group of neurons [32] - see Figure 1-7. It is important to mention that the term persistent activity does not only describe a period of constant elevated firing frequency. While the concept is that the firing frequency is above the neuronal baseline and does not completely disrupt during the delay period, dynamical behaviors like linearly increasing or decreasing forms are included.

In contrast to the prevailing theory of persistent activity, researchers have also developed a different theory that indicates sparse activity of neurons in the delay period and see the storage of information in hidden states rather than directly in neuron activity. An important argument is that older experiments used averaging techniques across neurons and even across trials which simplifies complex spiking dynamics and gives it a much smoother picture than it actually has [33]. Modern experiments with more accurate measuring possibilities show a much more dynamic and sparse spiking behavior compared to a simple persistent activity. Additionally, the oculomotor delayed-response task as an experiment itself for working memory has been criticized due to the inability to differentiate between actual short-term storage

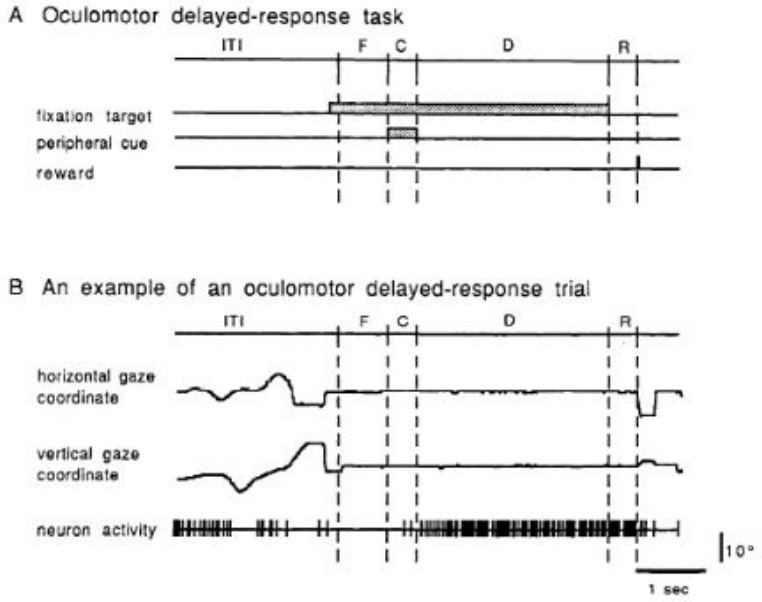

Figure 1-7: Persistent Neuronal Activity during Oculomotor Delayed Response Task [4]: Recording of neurons via electrodes during the working memory task showed tuned persistent activity in the prefrontal cortex of primates.

of input data and neuronal activity for motor planning. Alternatively, matching tasks and change detection can provide experimental results without any influence of motor planning. These modern experiment techniques give measurements that show sparse, synchronous spiking behavior rather than persistent enhanced activity [33].

Besides the experimental discrepancies, there are two important theoretical arguments that oppose the idea of mere persistent activity during the delay period. Firstly, the energy consumption due to persistent spiking presents a major problem. About a fifth of a human's energy consumption comes from the brain and its neuronal activity. It is doubtful that working memory functions who are basically omnipresent throughout our daily life rest upon such an energy intensive mechanism. Additionally, interruptions of the persistent activity would lead to the loss of information stored in the working memory leading to either a system prone to failure or to more redundancy regarding the information encoding which itself would increase the energy consumption even more [34].

Experimental results and theories about how input data is encoded have been mentioned but the underlying pathways enabling the neurons or hidden states to store the data without any input during the delay period have been left out. The most natural pathways for persistent activity is based on recurrent synaptic connections which assumes that connections between neurons activated during the stimulus phase are strong enough to continue the stimulus-specific spiking while simultaneously the connections to neurons not affected by the original stimulus are weak enough ensuring little information is lost. A prominent neuronal network model was published by [35] showing bistable neuronal activity during the simulation of a working memory experiment based on structured connectivity that emphasized on a strong decrease connected to spatial distance.

An alternative theory suggests intrinsic neuronal cell properties as the fundamental pathway of persistent activity. Due to experimental results showing persistent activity even in the case of disrupted synaptic neuronal circuits it has been concluded that neurons are able to act as integrators. An underlying mechanism is found in the CICR process of calcium similar to the calcium dynamics in astrocytes - see Section 1-2-3 [36].

A third possible pathway is constituted by STP which describes the change of synaptic strength and dynamics in the range of seconds. It is important to distinct this mechanism from long-term synaptic plasticity as the latter mechanism includes structural changes which are not present in working memory processes. A possible pathway for short-term synaptic facilitation is given by calcium residuals in presynaptic terminals which enhances the spiking probability. Calcium ions in the presynaptic terminal are necessary for the release of neurotransmitter and due to the slow degradation of calcium in the presynaptic terminal, following action potential can have an enhanced effect due to higher vesicle release compared to the first action potential if the following APs have a short enough inter-spike interval [37].

Lastly, astrocytic gliotransmission - as a second STP mechanism - provides a possible explanation for short-term synaptic facilitation in the range of several seconds. Astrocytes respond to neurotransmission in linked synapses with intracellular calcium oscillation which again can induce the release of gliotransmitter into the synaptic cleft. Possible effects on both presynaptic and postsynaptic terminals can increase or decrease the synaptic strength. Due to its slow but long-lasting dynamics - at least compared to neuronal dynamics - calcium oscillation can serve as a sort of preservation of action potentials.

1-3 Objectives and Contribution

In order to bring more insight into a possible astrocytic WM mechanism, two main steps are take to tackle this task from a control engineer's perspective. Firstly, mathematical cell models are reviewed and a tripartite model that itself consists of several cellular models is selected and analyzed with regard to its stability and neuronal firing behavior. This selection process is based on the requirements and significance of existing literature. A large amount of model description - especially for neurons - are given with strongly varying complexity and biological accuracy. The main compromises consist of model complexity and neglecting of less important pathways.

Secondly, the results obtained via the tripartite model analysis are verified via numerical simulation of a large-scale neuron/astrocyte network model. Numerical analysis allows higher biological accuracy due to less rigid mathematical limitations while a coherence with the individual tripartite model is preserved.

In this context, it is important to highlight the results of existing literature upon which the master thesis partly rests. In [38], the stability analysis of the Li/Rinzel model has been analyzed and bifurcation analysis of local equilibrium stability shows the limits of the

Li/Rinzel model regarding IP_3 input. In [39], a leaky integrate and fire formalism for an astrocyte has been introduced in order to build up a simplistic neuron-astrocyte network. The corresponding astrocytic firing enhances the synaptic release probability. In that way a network consisting of both inhibitory as well as excitatory neurons in combination with astrocytes has been created. This WM model shows persistent neuronal activity under the presence of gliotransmission which can not be detected in its absence.

Further on, detailed neuronal and astrocytic cell models are combined to form a realistic biological network in [5]. Gliotransmission on the presynaptic neuron and postsynaptic neuron has been summed in a synaptic efficacy. Numerical simulations have been studied - a single item and a multi item scenario - and the results show a well-functioning WM model with sparse neuronal activity. In this setting, no persistent firing activity has been shown during the delay period of the WM phase.

Additionally, in [40] simulations of a novel network model including astrocytes and neurons has been analyzed. The release of lysophosphatidic acid (LPA) by astrocytes has been considered the main pathway to enhance presynaptic release probability. For this purpose, the calcium dynamics have been modelled according to [37]. While the neuronal and astrocytic cell behavior is modelled rather simple, two STP pathways are combined. Besides the presynaptic calcium dynamics which on itself already portrays a possible WM mechanism, astrocytic gliotransmission impacting the presynaptic release mechanism is added. Additionally, the effect of noise for simulation scenarios with different parameters have been investigated. The results show that the network model displays a variety of neuronal activity including sparse, transient and persistent firing. Most importantly, it has been shown that the astrocytic layer adds a robustness component to the WM model that has been lacking before.

The contribution of this mast thesis lies in the novel stability analysis of a tripartite synapses with special regard towards the firing activity of the postsynaptic neuron. Slow inward currents have been selected as the primary method for gliotransmission. Secondly, focus is set on connecting sparse and persistent neuronal activity which have both been detected in WM experiments. Lastly, the numerical verification via the neuron-astrocyte network is build in a flexible way that allows easy investigation of specific tuning parameters such as neuron-astrocyte ratio.

In that manner, this master thesis provides further knowledge on the influence of astrocytes on postsynaptic neuronal spiking and supports astrocytic gliotransmission as a possible pathway for working memory supporting the seemingly contradictory theories of persistent and sparse firing during the delay period.

1-4 Outline

The structure of the thesis report is given as follows. Chapter 1 provides an introduction and motivation for research on the astrocytic influence on neural networks and memory processes. Following, Chapter 2 reviews the mathematical modelling of the tripartite synapse. In Chapter 3 the stability analysis of the tripartite model is performed. Finally, in Chapter 4

the simulation results of a realistic neuron-astrocyte network model in the context of working memory are shown.

Chapter 2

Modelling

In this chapter, the tripartite synapse model is presented. For that purpose, neuron and astrocyte models are described and its connection within the tripartite synapse is clarified.

2-1 Components of the Network Model

Mathematical models can be used to describe, analyse and simulate the behavior of biological cells. There is a wide variety of models for both neurons [41] and astrocytes [42] depending on the research focus and on the detailed dynamics that are supposed to be described. Figure 2-1 shows the basic structure of a tripartite synapse which is the sub-component that builds up the later neuron-astrocyte network model. Besides the cell models itself there are various formulations of their connections in the literature.

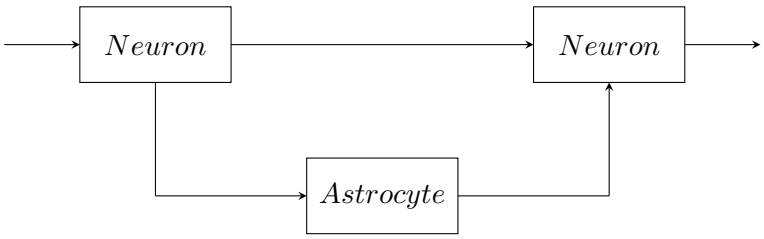

Figure 2-1: Tripartite Synapse: Depicted is the most basic structure of the tripartite synapse. The number of realizations with different sub-models are abundant.

The models used for the following steps are mainly based on the paper [5] whose focus lies already on the possible preservation of information by astrocytic dynamics. It combines the necessary biological accuracy with dynamics that are simple enough for large-scale simulation. In the following the modelling choices for the main sub-components are reviewed.

2-1-1 Neuron Model

Neuronal models have a long research history dating back to the first Integrate & Fire model by [43] more than a century ago. In principle neuronal models can be classified in conductance-based models such as the Hodgkin & Huxley model [44] and more abstract, phenomenological models such as the Izhikevich model [45]. The immense amount of research about neuronal modelling leads to a large list of models with varying accuracy and mathematical properties.

The decision of [5] to use the Izhikevich model is taken over as the model combines accurate display of fast firing dynamics - which is dominant in the PFC - as well as rather simple dynamics having only 2 differential equations. A notable drawback is the hybrid nature of the model that will create challenges for the mathematical analysis of the model. The continuous dynamics of the neurons are given by the following equations

$$\begin{array}{l} \frac{dV}{dt} = 0.04V^2 + 5V - U + 140 + I_{\text{app}} + I_{\text{syn}} + I_{\text{astro}} \\ \frac{dU}{dt} = a\left(bV - U\right) \end{array} \tag{2-1}$$

and the reset dynamics in case of an action potential being described as

$$\text{if } V \geq 30\text{mV, then } \begin{cases} V \leftarrow c \\ U \leftarrow U + d \end{cases} \tag{2-2}$$

with V denoting the membrane potential and U a membrane recovery variable which is connected to specific ion channel dynamics shortly after the voltage peak. The parameters a, b, c and d can be chosen in order to model different spiking behaviors such as tonic spiking, bursting or adaptive behavior. In this case, fast spiking neuronal behavior is selected according to the common type of neurons in the PFC. An overview of tested scenarios can be seen in [45] and the detailed parameter values can be seen in the Appendix A. The three mentioned currents I_{app}, I_{syn} and I_{astro} represent the applied current due to external stimulation, the synaptic current from other neurons and the astrocytic current due to glutamate release. The synaptic current is modelled in the following way [5]

$$I_{\text{syn}} = \sum_{k=1}^{N_{in}} \frac{\eta_{syn}\left(E_{\text{syn}} - V\right)}{1 + \exp\left(\frac{-V_{\text{pre}}^k}{k_{\text{syn}}}\right)} \tag{2-3}$$

which consists of a sum of all incoming synaptic current depending on all presynaptic voltages V_{pre}^k and the current V. In this way, the current voltage value of the postsynaptic neuron is taken into account as additional input. Current flow during an action potential of the postsynaptic neuron has in principle no effect as the ion channels are already activated. Recovery dynamics are not included in I_{syn} since they are already captured by the state U.

In order to give a better impression about the dynamics of this neuron model, simulation results are plotted in Figure 2-2a. In the left image, the state evolution of V can be seen for two different input values I_{app}. The unexcited neuron converges to a resting potential at $V_{rest} = -70V$ and does not show any AP. Under the influence of a stimulation current $I_{app} = 5\mu A$ regular firing occurs. The slightly different peak values can be explained by a nonzero simulation time step - more information about numerical integration in the Appendix

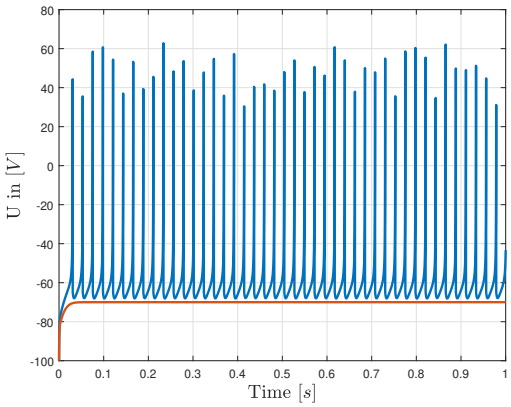

(a) Neuronal Dynamics of Izhikevich Model

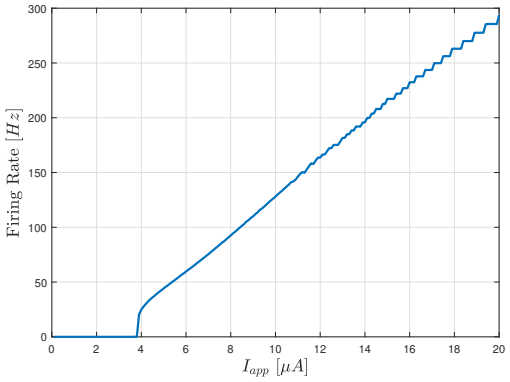

(b) Firing Frequency of the Izhikevich Model w.r.t. Input Strength I_{app}

Figure 2-2: Temporal Dynamics and Input-Current Dynamics of the Izhikevich Model according to Equation 2-1 and the parameters in Table A-3: In the left, the evolution of the membrane voltage is shown for two different stimulating input currents. Building upon this, the right figure shows the relation between input current and the average firing frequency in an interval of $I \in [0\mu A, 10\mu A]$ and a step size $\Delta I = 0.1\mu A$.

B. In the right image, the influence of the stimulation current is visualized. The neuron model belongs to class 2 neurons which demonstrate a sudden onset of neuronal spiking with a initial firing frequency f_0 significantly larger than zero. Class 1 neurons don't display a sudden onset jump but a continuous behavior. Here, there is a jump-like firing onset at a threshold $I_{thr} \approx 3.9\mu A$ which is clearly visible in the plot. After the onset, the linear relation between the firing frequency f and the applied current I_{app} is remarkable. All simulations are executed corresponding to Equation 2-1 with $I_{syn} = 0$ and $I_{astro} = 0$.

In addition to the standard Izhikevich model, the neuronal release dynamics of the neurotransmitter glutamate are described in the following, rather simple way [46],

$$\frac{dG}{dt} = -\alpha_{\text{glu}} G + k_{\text{glu}} \Theta\left(V - 30mV\right) \tag{2-4}$$

with Θ denoting the Heaviside step function and G denoting the amount of glutamate in the synaptic cleft. Since glutamate is the neurotransmitter with by far the most research and experimental results regarding astrocytic responses, it is the main mechanism in this tripartite model. In the following figure, the simulation results of the dynamics described above are shown with two constant spike trains as inputs - $f_1 = 50Hz$ and $f_2 = 125Hz$.

The simulation results in Fig 2-3 show the exponential decay during the spikes. Naturally, the "steady-state" value - as far as it is possible to name it like that - depends on the firing frequency and is reached roughly after 0.3 to 0.4 seconds. This "steady-state" value becomes important for the astrocyte input as it is described in the following section.

Originally, it has been intended to introduce additional synaptic dynamics - similar to [47] that take the availability of calcium ions and neurotransmitter vesicles near the presynaptic terminal into account. Unfortunately, the fast-spiking neurons have not yet been examined

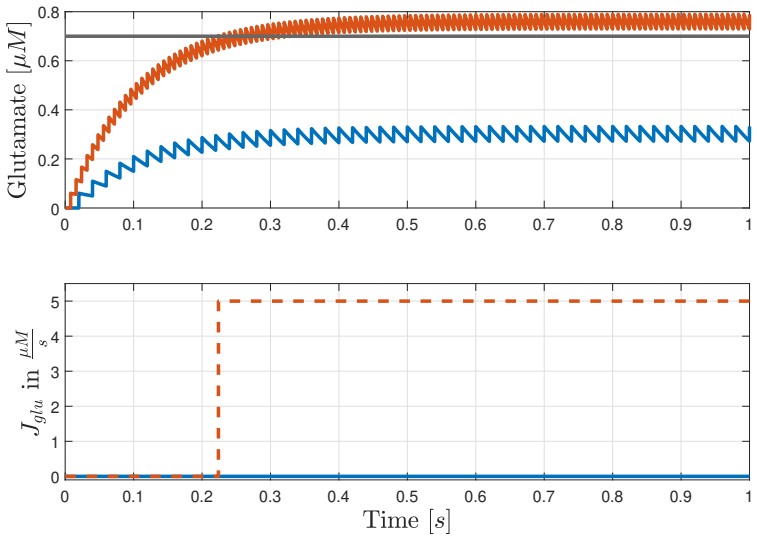

Figure 2-3: Glutamate Dynamics: The glutamate dynamics according to equation 2-4 are shown for two different uniform spike trains.

with respect to this mechanism or at least reliable parameter values are not available in reviewed literature. In [47], the authors have based their model on firing rates between 10 and 25Hz while firing rates of more than 100Hz are not uncommon for the scenarios described in this thesis. As already mentioned in section 1-3 the presynaptic calcium dynamics are one possible mechanism of short-term information storage which would have made their inclusion very informative.

2-1-2 Astrocyte Model

In contrast to the modelling of neurons, astrocyte models have not such a huge amount of experimental background and variety. Although [42] gives a review of a large number of existing astrocyte models, it has to be mentioned that a great amount of these models share the same base models and consist only of slightly different adaptions or simplifications. The most common and largely accepted model for calcium dynamics is given by Li/Rinzel [48] as a simplification of [49] which form a foundation for most of astrocyte models. A common modification is the extension by a third state describing the IP_3 dynamics and making it more applicable for inputs and simultaneously considering the non-rigid nature of IP_3. Additionally, models based on [50] and [51] are present in the literature but they are slightly less used in modern research literature [42].

Similarly to the neuronal dynamics, the modelling of the astrocyte dynamics, for this thesis project, is taken over by [5]. Compared to other astrocyte models like [51] and [52], the given model provides relatively simple dynamics while including all major mechanisms. A further argument for this model is the possibility for neuron to astrocyte as well as astrocyte to astrocyte connections. The continuous dynamics of the astrocyte is given by a Li/Rinzel model with modification by [25] and [53] and can be described by the following differential

equations

$$\begin{aligned}
\frac{d\left[\mathrm{IP_3}\right]}{dt} =& \frac{IP_3^* - \left[\mathrm{IP_3}\right]}{\tau_{IP3}} + \frac{v_4\left(\left[\mathrm{Ca^{2+}}\right] + (1-\alpha)k_4\right)}{\left[\mathrm{Ca^{2+}}\right] + k_4} + J_{\mathrm{glu}} + \mathrm{diff}_{IP3} \\
\frac{d\left[\mathrm{Ca^{2+}}\right]}{dt} =& c_1 v_1 \left[Ca^{2+}\right]^3 h^3 \left[\mathrm{IP_3}\right]^3 \frac{\left(c_0/c_1 - (1+1/c_1)\left[Ca^{2+}\right]\right)}{\left(\left[\mathrm{IP_3}\right] + d_1\right)^3 \left(\left[\mathrm{Ca^{2+}}\right] + d_5\right)^3} - \frac{v_3 \left[Ca^{2+}\right]^2}{k_3^2 + \left[Ca^{2+}\right]^2} \\
&+ c_1 v_2 \left(c_0/c_1 - (1+1/c_1)\left[\mathrm{Ca^{2+}}\right]\right) + \frac{v_6 \left[\mathrm{IP_3}\right]^2}{k_2^2 + \left[\mathrm{IP_3}\right]^2} - k_1\left[Ca^{2+}\right] + \mathrm{diff}_{\mathrm{Ca}} \\
\frac{dh}{dt} =& a_2\left(d_2 \frac{\left[\mathrm{IP_3}\right] + d_1}{\left[\mathrm{IP_3}\right] + d_3}(1-h) - \left[Ca^{2+}\right] h\right)
\end{aligned} \tag{2-5}$$

with the states $\left[\mathrm{IP_3}\right]$, $\left[\mathrm{Ca^{2+}}\right]$ and h denoting the concentration of IP_3 and Ca^{2+} inside the astrocytic cytoplasm as well as the share of active IP_3 receptors. This three-dimensional, nonlinear system describes the calcium dynamics of an astrocyte.

The diffusion terms, denoted by $\mathrm{diff}_{Ca/IP3}$, represent the Ca^{2+} and IP_3 flows caused by diffusion across the astrocytic syncytium via gap junctions. These dynamics are excluded within the tripartite synapse due to the lack of a second astrocyte and are examined in more depth in the following subsection.

The input J_{glu} describes the transmitter induced IP_3 production and is thus the connection between presynaptic neuron and astrocyte. The mechanism is defined in the following way

$$J_{\mathrm{glu}} = \begin{cases} A_{\mathrm{glu}}, & \text{if} \quad t_0 < t \leq t_0 + t_{\mathrm{glu}} \\ 0, & \text{otherwise} \end{cases} \tag{2-6}$$

with t_0 denoting the latest time stamp when the glutamate level exceeds a threshold value $G_{thr} = 0.7\mu M$ which leads to a pulse-shaped IP_3 production of amplitude A_{glu} and duration t_{glu} if more than $F_{act} = 50\%$ of the connected neurons exceed the glutamate level a the same time. The pulse-shaped J_{glu} is independent of any other parameter. The mathematical equation for this condition is given here

$$\left(\frac{1}{N_a}\sum_{(i)\in N_a}\left[G^{(i)} > G_{thr}\right]\right) > F_{act} \tag{2-7}$$

which translates to the fact that more than half of the connected neurons have to release enough glutamate for an astrocytic reaction in the form of IP_3 production. The simulation results of the glutamate dynamics in Figure 2-3 shows that the required neuronal firing frequency is quite high for the surpassing of G_{thr}.

Lastly, a short simulation of the astrocyte model is portrayed in Figure 2-4 in order to give a picture of the dynamics. Two input signals - a short initial and a persistent constant signal - are applied to the astrocyte. The dynamics of both scenarios show very similar behavior within the first 4 seconds. Especially, the calcium oscillation as a reaction to the glutamate induced IP_3 production is characteristic. The long-lasting astrocyte dynamics compared to

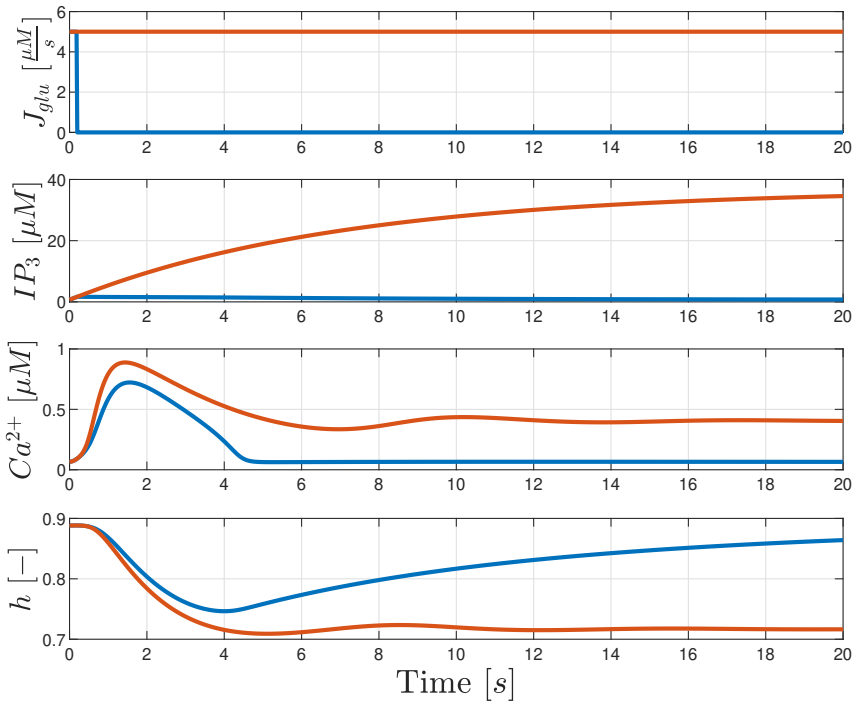

Figure 2-4: Astrocyte Dynamics according to [25]: The simulation of the astrocyte model exposed to two different input signals is shown. While the short input signal is characteristic for working memory experiments with a short stimulation, the persistent signal shows the steady-state solution after a while.

the short J_{glu} pulse which can be correlated to a short firing sequence shows promising results for a possible way for information storage during neuronal quiescence. Naturally, the steady-state response of both system is slightly different. It should be mentioned that the initial value for the simulation corresponds to the equilibrium value of the unperturbed astrocyte model.

2-1-3 Miscellaneous Model Components

An important difference to the model by [5] is the feedback mechanism that is used. Instead of enhancing the efficacy of the synaptic transmission due to higher glutamate release which is linked to activation of presynaptic receptors [3] - as it can be seen in the equation below,

$$\begin{aligned} g_{\text{syn}} &= \eta + v_{Ca} \\ v_{Ca} &= v_{Ca}^{*} \Theta \left(\left[Ca^{2+} \right]^{(m,n)} - \left[Ca^{2+} \right]_{\text{thr}} \right) \end{aligned} \tag{2-8}$$

the focus lies on slow inwards currents induced by activated NMDA receptors at the postsynaptic neuron. The formulation is taken from [25], giving

$$\begin{aligned} I_{\text{astro}} &= 2.11 \Theta(\ln y) \ln y \\ y &= \left[\text{Ca}^{2+} \right] / \text{nM} - 196.69 \end{aligned} \tag{2-9}$$

with $\Theta(x)$ denoting in both cases the Heaviside function. It should be mentioned that the old threshold value $\left[Ca^{2+} \right]_{\text{thr}} = 0.15 \mu M$ is significantly lower than for the new feedback mechanism. In practice, this change means that instead of enhancing the effect of action potentials, postsynaptic neurons are slightly easier to excite in a more continuous way and the astrocytic feedback strength is independent of future action potentials of the presynaptic neuron.

Although the classic tripartite synapse includes only one astrocyte, the connection mechanism for the astrocytic syncytium are shown here as these links are an important feature of the neuron-astrocyte network model. Gap junctions enable both IP_3 molecules as well as Ca^{2+} the flow between astrocytes. The modelling approach is taken over by [5] due to its simplicity:

$$\begin{aligned} \text{diff}_{Ca} &= d_{Ca} \left(\Delta \left[Ca^{2+} \right] \right) \\ \text{diff}_{IP3} &= d_{IP_3} \left(\Delta \left[\text{IP}_3 \right] \right) \end{aligned} \tag{2-10}$$

with the Δ operator denoting the sum of the concentration differences with respect to all neighboring astrocytes. Consequently, the strength of the inter-astrocyte exchange is proportional to their concentration difference. A second pathway of astrocytic interconnection based on ATP - as described in Section 1-2-2 - has been neglected due to the required modelling complexity. The literature review has shown that only little research on the influence of astrocyte-to-astrocyte connections in the context of working memory has been conducted to this point.

2-2 Tripartite Synapse

Combining the sub-models in the structure shown in Figure 2-1, the following state space system is formulated:

$$\dot{x} = \begin{bmatrix} \dot{x}_1 \\ \dot{x}_2 \\ \dot{x}_3 \\ \dot{x}_4 \\ \dot{x}_5 \\ \dot{x}_6 \\ \dot{x}_7 \\ \dot{x}_8 \end{bmatrix} = \begin{bmatrix} 0.04x_1^2 + 5x_1 - x_2 + 140 + I_{\text{app},1} \\ a\left(bx_1 - x_2\right) \\ -\alpha_{\text{glu}} x_3 + k_{\text{glu}} \Theta\left(x_1 - 30mV\right) \\ \frac{IP_3^* - x_4}{\tau_{IP3}} + \frac{v_4(x_5 + (1-\alpha)k_4)}{x_5 + k_4} + J_{\text{glu}} \\ c_1 v_1 x_5^3 x_6^3 x_4^3 \frac{(c_0/c_1 - (1+1/c_1)x_5)}{((x_4+d_1)(x_5+d_5))^3} - \frac{v_3 x_5^2}{k_3^2 + x_5^2} + c_1 v_2 \left(c_0/c_1 - (1+1/c_1)\, x_5\right) + \frac{v_6 x_4^2}{k_2^2 + x_4^2} - k_1 x_5 \\ a_2 \left(d_2 \frac{x_4 + d_1}{x_4 + d_3}\left(1 - x_6\right) - x_5 x_6\right) \\ 0.04x_7^2 + 5x_7 - x_8 + 140 + \frac{\eta_{syn}(E_{\text{syn}} - x_7)}{1 + \exp\left(\frac{-x_1}{k_{\text{syn}}}\right)} + I_{astro} \\ a\left(bx_7 - x_8\right) \end{bmatrix}$$

with additional update equation for neuronal spiking - see Equation 2-2 - for the presynaptic and the postsynaptic neuron, glutamate dependent IP_3 production in equation 2-6 and astrocytic gliotransmission in the form of I_{astro} in Equation 2-9. The states denote the following physical values:

x_1	membrane voltage of the presynaptic neuron
x_2	recovery variable of the presynaptic neuron
x_3	concentration of released glutamate
x_4	concentration of IP_3 inside the astrocyte
x_5	concentration of Ca^{2+} inside the astrocyte
x_6	share of activated IP_3 receptors at the astrocyte's ER
x_7	membrane voltage of the postsynaptic neuron
x_8	recovery variable of the postsynaptic neuron

Table 2-1: Overview of States - Tripartite Synapse

describing a tripartite synapse using an eight-dimensional nonlinear and hybrid state space system with over 20 different parameters.

Chapter 3

Analysis of the Tripartite Model

In this section, the stability of a simplified tripartite synapse is analyzed and numerically verified. While the state-space system according to Equation 2-2 will be used for the simulation of a large-scale neuron-astrocyte network, a stability analysis for such a complex model has proven to not be feasible in scope of this master thesis.

3-1 Problem Formulation

In Section 1-2-3, the existence of two competing theories namely the persistent and sparse activity during working memory task is introduced and elucidated. The objective of this thesis project is to give theoretical evidence for astrocytic gliotransmission as a possible pathway for working memory tasks showing both persistent activity and sparse activity.

Following this hypothesis, astrocytic calcium dynamics and the corresponding gliotransmission act as the hidden state - as it is described within theory of sparse activity - while the possible occurrence of persistent activity relies on the strength of the gliotransmission. Consequently, astrocytic feedback to neurons will be applied as a tuning parameter determining whether persistent or sparse activity takes place during the delay memory phase. In order to give evidence for a possible astrocytic working memory pathway, the synaptic model is analyzed in this section. Furthermore, simulation for both the synaptic model as well as the neuron-astrocyte network model are performed to test the hypothesis in the following chapter. The results of various simulation scenarios imitating working memory experiments with animals are shown.

The concrete idea is to analyse the equilibrium values of a simplified tripartite synapse in order to draw conclusions regarding the neuronal firing of the postsynaptic neuron for no gliotransmission, weak gliotransmission and strong gliotransmission. It is hypothesised that the strength of gliotransmission act as the decisive parameter for the occurrence of persistent activity. Stability analysis of the equilibria validates the significance of the conclusions as it

proves that the cell model actually reach and remain the state.

3-2 Stability Analysis

In order to analyze mathematically gliotransmission and its effect, only parts of the state space model - namely the astrocyte dynamics captured in the states x_{4-6} - are considered in the following. The reason for this step is the complexity of analyzing a high-dimensional, nonlinear and hybrid model. Denoting this new state space system $\dot{x}^*$ and defining it as:

$$\dot{x}^* = \begin{bmatrix} \dot{x}_1^* \\ \dot{x}_2^* \\ \dot{x}_3^* \end{bmatrix} = \begin{bmatrix} \dot{x}_4 \\ \dot{x}_5 \\ \dot{x}_6 \end{bmatrix} \tag{3-1}$$

which consists of only three continuous but nonlinear differential equations. Additionally, an auxiliary firing state x_4^* is introduced to examine the effect of gliotransmission on postsynaptic neuronal spiking. The corresponding state space is given as follows

$$\mathbb{X}^* = \{x^* \in \mathbb{R}^+ \,|\, 0 \leq x_3^* \leq 1\} \tag{3-2}$$

which is defined by physically feasible boundaries, meaning negative concentrations as well as negative firing rates are not included. On top of that, the share of activated IP_3 receptors in ER logically has a value range of $[0, 1]$.

In principle, the following block diagram describes the cascade connection between the astrocyte and the postsynaptic neuron in an illustrative way.

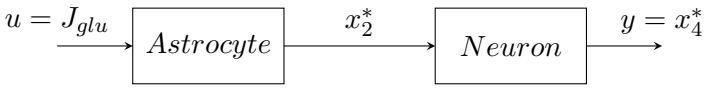

Figure 3-1: Extended Astrocyte Model

Derivation of the firing state

The dynamics of the firing state x_4^* are derived in the following way using the known relation of the Izhikevich model between input current and firing frequency as depicted in Figure 2-2b. The Izhikevich model clearly shows a ON/OFF behavior regarding its firing frequency. Applying an approximate input current $I_{app} \leq I_{thr} \approx 3.9\mu A$ leads to neuronal firing activity whose magnitude has a approximately linear correlation to I_{app}. For the extended astrocyte model, it is assumed that no additional external input is exciting the postsynaptic neuron and the slow inward currents caused by astrocytic gliotransmission provides the sole excitation of the postsynaptic neuron, thus $I_{app} = I_{astro}$. The firing frequency is described by the following equation:

$$\dot{x}_4^* = -x_4^* + f(I_{astro}) \tag{3-3}$$

with

$$f_1(I_{astro}) \approx \Theta(I_{astro} - I_{thr})(p_1 I_{astro} + p_2) \tag{3-4}$$

where the Θ function models the sudden start of the firing and the linear term approximates the observed correlation. The parameters $p_1 = 16.82$ and $p_2 = -40.29$ have been acquired via the linear least square method. In order to perform simple analysis, the current hybrid equation has to be modified into a continuous equation. For that purpose the tanh function is used to replace the non-continuous Θ function leading to the following expression.

$$\dot{x}_4^* = -x_4^* + \frac{1}{2}(\tanh(\eta I_{astro} - I_{thr}) + 1)(p_1 \eta I_{astro} + p_2) \tag{3-5}$$

with $\eta \in [0, 1]$ denoting the efficacy of gliotransmission. Additionally, the astrocytic current I_{astro} which is described in Equation 2-9 is approximated by a continuous function. The term

$$I_{astro}(x_2^*) = 2.11\Theta(\ln y) \ln y, \quad y = [x_2^*]\,/\mathrm{nM} - 196.69 \tag{3-6}$$

is approximated in a similar way as above using a tanh function in order to obtain the following expression

$$f(x_2^*) = a \tanh(b x_2^* + c) + d \tag{3-7}$$

in a realistic range of calcium values $x_2 \in [0.05, 0.7]\ \mu M$. The parameter fitting for $a = 6.3611$, $b = 14.682$, $c = -3.3582$ and $d = 6.3611$ has been executed via Matlab. As it can be seen in Figure 3-2, the qualitative development of I_{astro} is captured although considerable error is visible at the onset due to the smoothing process. Lastly, a very small valued addend $\epsilon = 0.02$ is included in order to account for small negative values in the low input due to simplification errors which leads to the following equation:

$$\dot{x}_4^* = -x_4^* + \frac{1}{2}(\tanh(\eta I_{astro} - I_{thr}) + 1)(p_1 \eta I_{astro} + p_2) + \epsilon \tag{3-8}$$

This concludes the derivation of the extended astrocyte model $\dot{x}^*$.

$$\dot{x}^* = \begin{bmatrix} \dot{x}_1^* \\ \dot{x}_2^* \\ \dot{x}_3^* \\ \dot{x}_4^* \end{bmatrix} = \begin{bmatrix} \dot{x}_4 \\ \dot{x}_5 \\ \dot{x}_6 \\ -x_4^* + \frac{1}{2}(\tanh(\eta I_{astro} - I_{thr}) + 1)(p_1 \eta I_{astro} + p_2) + \epsilon \end{bmatrix} \tag{3-9}$$

Equilibrium States

The equilibrium or steady state values are compared for three different cases - as shown below. Case 1 and Case 2 are selected in order to demonstrate the active role of astrocytes as a storage of neuronal firing. Case 2 and 3 are present in order to point out the influence of gliotransmission on the postsynaptic firing activity. Due to the nature of steady state analysis, it is not possible to a analyse pulse-shaped input J_{glu} as it is realistically done in actual working memory experiments with animals. Instead these dynamics will be later shown by numerical analysis in Section 3-3. For the sake of mathematical analysis, it is assumed that the short period of actual stimulation is sufficient for the astrocyte model to approach the steady state value of the persistently stimulated case - at least for a limited period of time - which again will be supported in Section 3-3.

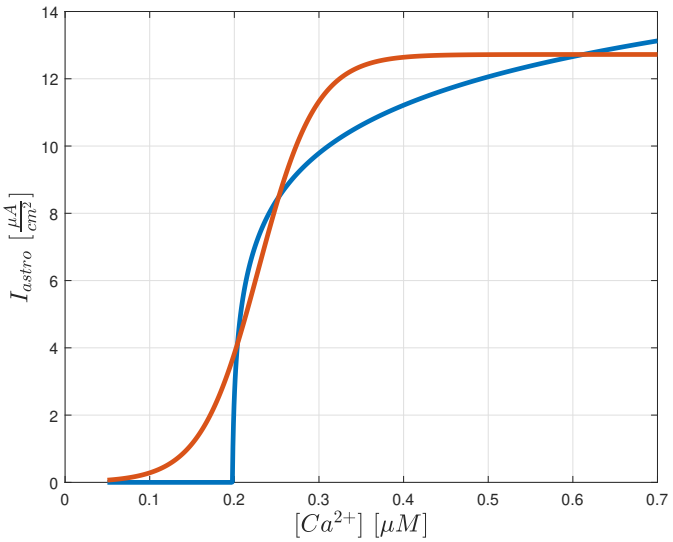

Figure 3-2: Estimation of I_{astro}: The hybrid relation between the calcium concentration and the astrocytic current is estimated by a tanh-function.

- Case 1: No stimulation of the astrocyte is present resulting into no glutamate induced IP_3 production $\rightarrow J_{glu} = 0$
- Case 2: Persistent stimulation of astrocyte due to persistent presynaptic spiking and strong astrocytic gliotransmission to the postsynaptic neuron $\rightarrow J_{glu} = 5$ and $\eta = 100\%$
- Case 3: Persistent stimulation of astrocyte due to persistent presynaptic spiking and weak astrocytic gliotransmission to the postsynaptic neuron $\rightarrow J_{glu} = 5$ and $\eta = 25\%$

Computing the equilibrium values x_0^* by solving $\dot{x}^* = 0$ leads to several possible solutions due to the nonlinearities. According to the state space $\mathbb{X}^*$ of the extended astrocyte model, all solutions including complex parts or negative parts are removed due to infeasibility. This leads to exactly one possible equilibrium state for each case:

Case	x_1^* **in** μM	x_2^* **in** μM	x_3^*	x_4^* **in Hz**
1	0.6858	0.06612	0.8882	0.0004924
2	36.77	0.4061	0.7165	172.5
3	36.77	0.4061	0.7165	2.427

Table 3-1: Overview of Equilibrium Values

As it can be seen in the table above, the equilibrium states for Case 1 and 2 differ significantly. Most noteworthy, the steady state calcium concentration x_2^* inside the astrocyte exceeds the threshold value for the astrocytic current which is $Ca_{thr,1}^{2+} = 0.19669\mu M$ for the original and $Ca_{thr,2}^{2+} = 0.2287\mu M$ for the continuous version. This demonstrates that astrocytes actively respond to presynaptic neuronal firing by internal calcium dynamics. From the equilibrium

value of x_4^*, the effect of astrocytic gliotransmission becomes also obvious. A large difference in neural activity can be seen between weak and strong gliotransmission.

Additionally, the difference in Case 2 and 3 shows the significance of strong astrocytic feedback. It has to be mentioned that $\eta_2 = 25\%$ is selected in a smart way in order to show maximum effect. If the weaker gliotransmission does not evoke a current $I_{astro} \geq I_{thr}$, the postsynaptic neuronal firing is strongly reduced and leads to sparse activity, although the astrocytic dynamics are the same as in case 2. Nevertheless, I_{astro} is still effecting the postsynaptic neuron and additional stimulation via a recall cue would lead to a much stronger neuronal response than without any astrocytic influence. This observation supports the idea that calcium dynamics could act as a storing mechanism of neuronal activity with the astrocytic gliotransmission causing sparse or persistent activity depending on the strength of astrocytic gliotransmission.

Local Stability Analysis

The computation of equilibrium states is only the first step in the model analysis. In order to actually draw the conclusions above, it must be guaranteed that the system approaches the equilibrium states meaning that the equilibrium states are stable and attracting in the local area that corresponds biological feasibility. It is important to mention that the system in the three cases is treated as an autonomous system by incorporating the constant input signals J_{glu} into the state dynamics. This allows the application of Lyapunov's indirect method as described in Theorem 3.2 of [54].

Theorem 3.2 [54]: Let $x = 0$ be an equilibrium point for the nonlinear system $\dot{x} = f(x)$, where f is continuously differentiable in a neighborhood of the origin. Let

$$A = \frac{\partial f}{\partial x}(x)\Big|_{x=0} \tag{3-10}$$

and denote its eigenvalues by λ_1 to λ_n. Then,

1. The origin is exponentially stable if and only if $\mathfrak{Re}\,[\lambda_i] < 0$ for all eigenvalues.
2. The origin is unstable if $\mathfrak{Re}\,[\lambda_i] > 0$ for one or more of the eigenvalues

Proposition 1. *The equilibrium of the nonlinear system for all three cases as described above are locally asymptotically stable.*

Proof. Let us compute the Jacobian of the nonlinear system. Since the system is continuously differentiable for all three cases, the Jacobian matrix A_i - as described above - is given as

$$A = \frac{\partial f(x^*)}{\partial x^*}\Big|_{x^*=x_0^*} = \begin{bmatrix} \frac{df_1(x^*)}{dx_1^*} & \frac{df_1(x^*)}{dx_2^*} & \frac{df_1(x^*)}{dx_3^*} & \frac{df_1(x^*)}{dx_4} \\ \frac{df_2(x^*)}{dx_1^*} & \frac{df_2(x^*)}{dx_2^*} & \frac{df_2(x^*)}{dx_3^*} & \frac{df_2(x^*)}{dx_4^*} \\ \frac{df_3(x^*)}{dx_1^*} & \frac{df_3(x^*)}{dx_2^*} & \frac{df_3(x^*)}{dx_3^*} & \frac{df_3(x^*)}{dx_4^*} \\ \frac{df_4(x*)}{dx_1^*} & \frac{df_4(x^*)}{dx_2^*} & \frac{df_4(x^*)}{dx_3^*} & \frac{df_4(x^*)}{dx_4^*} \end{bmatrix}\Bigg|_{x^*=x_0^*} \tag{3-11}$$

with the following matrices A_1, A_2 and A_3 denoting the Jacobian matrix for Case 1, 2 and 3.

$$A_1 = \begin{bmatrix} -0.14 & 0.19 & 0 & 0 \\ 0.42 & -4.3 & 1.4 & 0 \\ 0.0050 & -0.12 & -0.083 & 0 \\ 0 & 0.009 & 0 & -1.0 \end{bmatrix}$$

$$A_2 = \begin{bmatrix} -0.14 & 0.12 & 0 & 0 \\ 0.0006 & -0.33 & 7.80 & 0 \\ 0 & -0.10 & -0.20 & 0 \\ 0 & 7.1 & 0 & -1.0 \end{bmatrix}$$

$$A_3 = \begin{bmatrix} -0.14 & 0.12 & 0 & 0 \\ 0.0006 & -0.33 & 8.00 & 0 \\ 0 & -0.10 & -0.20 & 0 \\ 0 & 28.2 & 0 & -1.0 \end{bmatrix}$$

and the corresponding eigenvalues λ_{1-4} are given in the following table

Case	λ_1	λ_2	λ_3	λ_4
1	-4.2324	-0.12 + 0.023i	-0.12 - 0.023i	-1
2	-0.14	-0.27 + 0.89i	-0.27 - 0.89i	-1
3	-0.14	-0.27 + 0.89i	-0.27 - 0.89i	-1

Table 3-2: Eigenvalues of Jacobians

which confirms the local exponential stability of each equilibrium point and therefore, the convergence of the system to the equilibrium values within a small region. □

In [55], local boundaries regarding the region of attraction are defined using the positivity property of the nonlinear system without x_4 [56]. This concludes the mathematical analysis of the extended astrocyte model.

3-3 Numerical Verification

In order to confirm the results of the mathematical analysis and to obtain additional results, numerical simulations of the extended astrocyte model - see Figure 3-1 - and the tripartite synapse - see Figure 2-1 - are executed. The corresponding details for the algorithm and parameters regarding numerical simulation are explained in Appendix B.

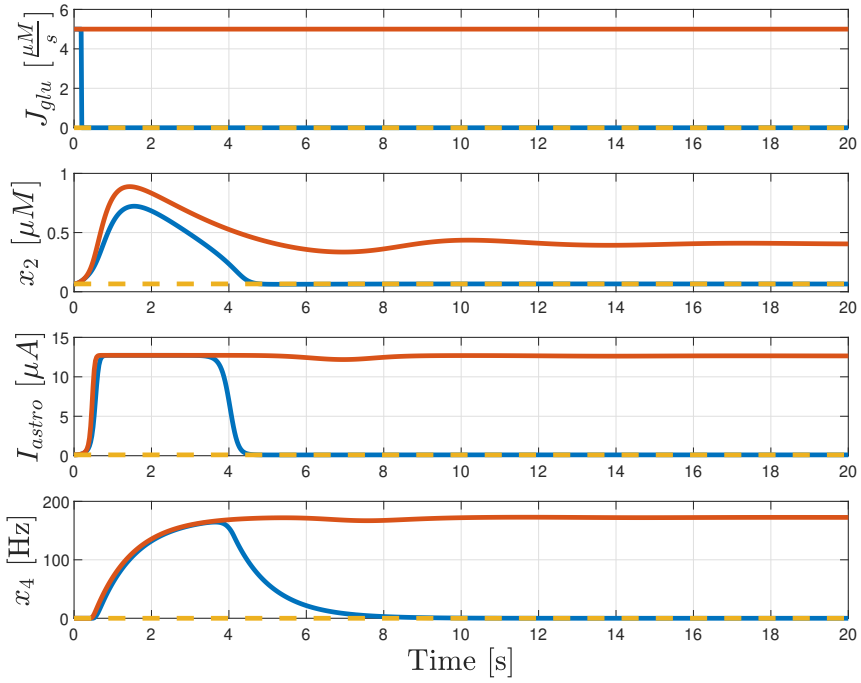

Figure 3-3: Numerical Results for Extended Astrocyte Dynamics: The extended astrocyte model is simulate using three different input signals. Case 1 with zero input signal is reflected in yellow while case 2 with a persistent input $J_{glu} = 5\frac{\mu M}{s}$ is given by in red. Additionally, a third scenario with a short input (blue) shows that the temporal behavior can be accurately estimated by the steady-state value of the excited astrocyte at least within the first 4 to 5 seconds.

In Figure 3-3, the simulation results for the extended astrocyte model is shown. Both Cases 1 and 2 as well as Case 2 with a time limited input of $\Delta t = 0.2s$ are simulated and plotted according to the legend in the fourth sub-figure. The calculated equilibrium states for x_2^* and x_4^* - as already shown in Table 3-1 - can clearly be confirmed and furthermore, the additional dynamics - shown in red - follow the dynamics with persistent input quantitatively very well. This confirms the assumption that the steady-state value reflects the temporal dynamics of the astrocyte model. Additionally, the difference between weak and strong gliotransmission is shown in Figure 3-4. While the calcium dynamics are completely identical, the effect on the firing rate differs greatly. The weak gliotransmission with $\eta = 25\%$ does not have any visible effect on the postsynaptic firing. In contrast, the strong gliotransmission leads to a notable response.

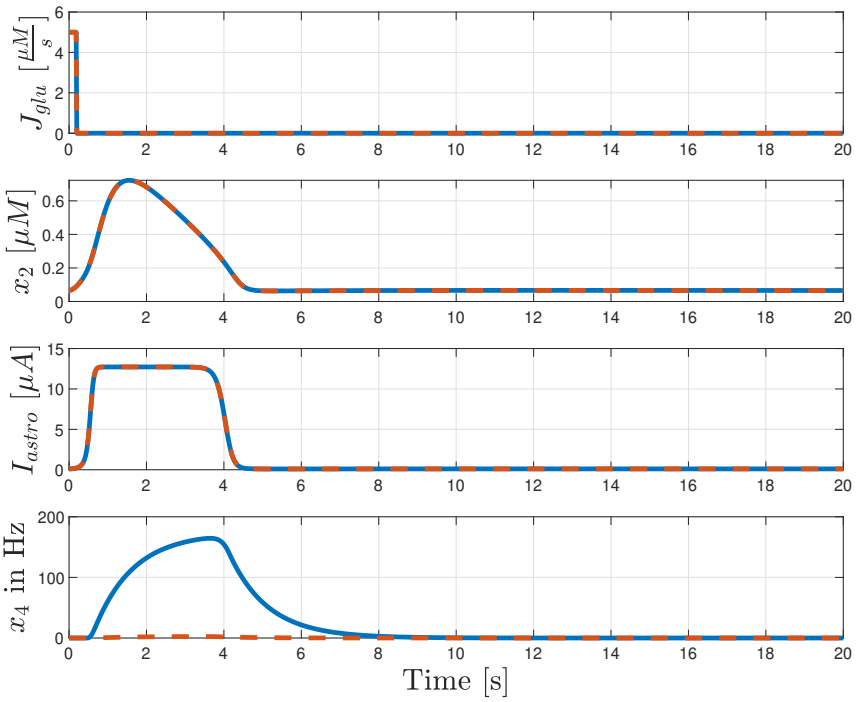

Figure 3-4: Numerical Results for Extended Astrocyte Dynamics: Simulating the model with a short impulse signal with weak (red) and strong (blue) gliotransmission demonstrates the immense effect of gliotransmission on the postsynaptic firing activity.

Finally, the numerical simulation results of the tripartite system - as described in equation 2-2 - are shown. In that way, the adequacy of simplifications within the extended astrocyte model is supported by coherent results of both models. More accurately, the tripartite synapse is shown for two scenarios - with a short ($\Delta t = 0.2s$) and a persistent input signal of $I_{app} = 100\mu A$. Most interesting are the temporal dynamics of the astrocyte compared to the steady state value which is already analyzed in the previous section 3-2. Similar to classical working memory experiments, a short stimulation phase of 0.2 seconds is followed by a delay phase of 2.8 seconds which is terminated by the recall phase - compare with [4], [14]. Analyzing the state evolution Ca^{2+} shows strong similarities for the first 4 to 5 seconds. Afterwards, the deviation becomes clear but until this points the response behavior to a short impulse and a persistent signal is very close. This proves the meaningfulness of the equilibrium analysis from Section 3-2. The neuronal dynamics are shown via the firing frequencies of the presynaptic f_1 and postsynaptic neuron f_2. The thickness in fourth graph is due to jumping behavior of the firing frequency f_2 which can be lead back to the computation of the average firing frequency within an interval $\Delta t_{fir} = 0.1s$. The firing frequency of the postsynaptic neuron clearly resembles the dynamics of the astrocytic current I_{astro}. The calcium dynamics in the lowest subplot also show that the storing effect of the gliotransmission is limited to around 5 seconds after the end of the input signal which corresponds to the temporal limits of working memory.

This concludes the stability analysis of the extended astrocyte and tripartite model regarding

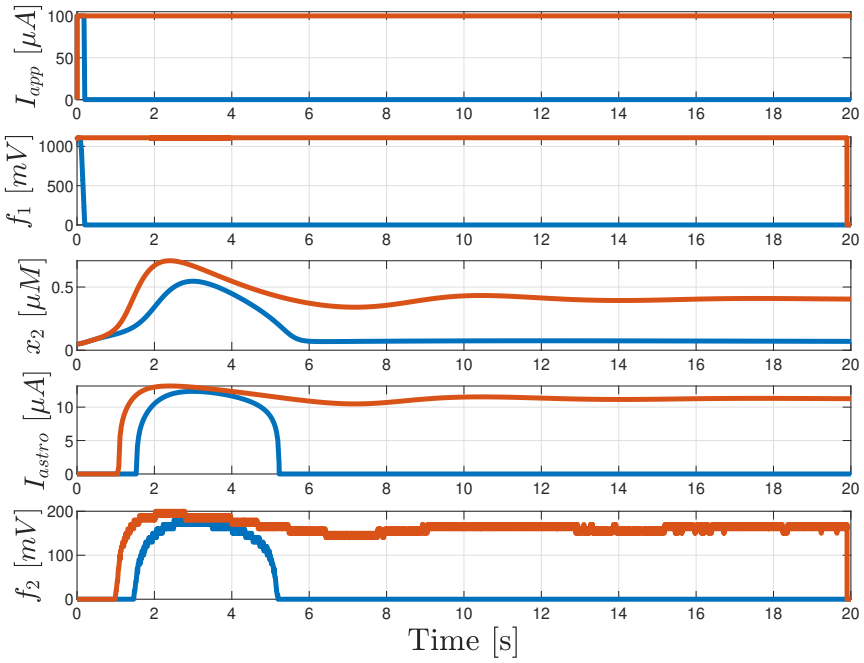

Figure 3-5: Numerical Results for Tripartite Synapse: The simulation of the tripartite synapse exposed to two different input signals is shown. While the short input signal is characteristic for working memory experiments with a short stimulation, the persistent signal shows the steady-state solution.

provoked neuronal activity and its significance in the context of WM.

Chapter 4

Simulating Working Memory

The goal of the following numerical simulations is to provide evidence for possible astrocytic feedback activity as a pathway for working memory. In order to support this hypothesis for the astrocytic mechanism both sparse and persistent activity are shown during the delay period in working memory tasks. The simulation scenarios are designed to imitate experiments with primates - see [4] or [14] - in order to be as realistic as possible.

In section 4-1, the details of the network architecture as well as the major parameters are presented. Different stimulation protocols are designed to show sparse and persistent activity which will be explained in detail in section 4-2. Besides the one-item recall task, a multi-item experiment is simulated giving rise to two further simulation protocols. In Section 4-3, the results for the different simulation protocols are shown and examined. Besides the regular simulation protocols, further simulations are conducted to examine the influence of gliotransmission, connectivity schemes and the neuron-to-astrocyte ration.

The network simulations are performed using Matlab with Runge-Kutta-Fourth-Order (RK4) algorithm and a simulation time step $\Delta t = 0.1\mu s$. Reasoning for the algorithm and parameter choice as well as the code structure itself can be found in the Appendix B.

4-1 Realistic Network

Building up on the tripartite synapse as described in Equation 2-2, a network model has been developed in order to execute different simulation scenarios in the context of working memory. The goal is to verify the possibility of storing information by astrocytic gliotransmission showing various spiking behavior. Analog to [5], the network model consists of two layers, a neuronal network layer and an astrocytic network layer that are interconnected in a structured way - see Figure 4-1. Both layers consist of a squared number of cells whose number is directly linked with each other. A standard ratio of neurons to astrocyte is chosen to be $r_{N-A} = 4$ but the simulation environment offers the possibility to decrease to $r_{N-A} = 1$

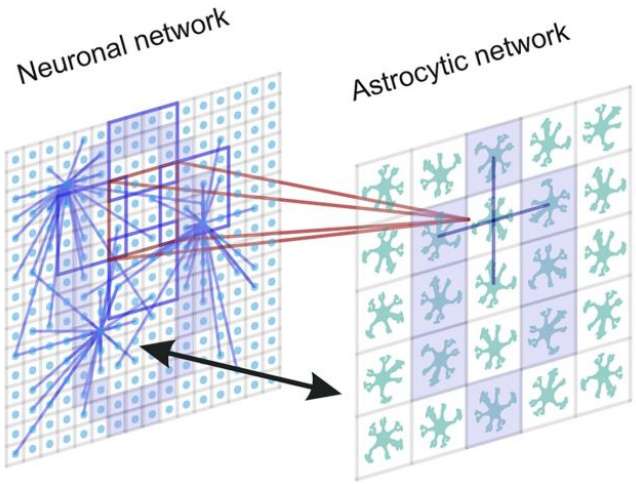

Figure 4-1: Dual Layer Network Structure [5]: The neuronal layer on the left and the astrocytic layer on the right form spatial interconnections. Additionally, the number zero is depicted to demonstrate the encoding of input as neuronal firing on the left and consequently as astrocytic calcium oscillations on the right.

or increase to $r_{N-A} = 9$.

The number of neurons is chosen by finding a compromise between low simulation time and high contrast between non-stimulated and stimulated neurons. A comprise is found at 1296 neurons - the square of 36 - and 324 astrocytes - the square of 18. The standard number of neurons enables an easy switching between the three possible r_{N-A} values. It is furthermore based on a comparison of different neuron-astrocyte models in the corresponding literature study.

The dynamics of chemical synapses between neurons have already been elaborated in the previous section, however to model biological accurate network dynamics it is clearly not desirable to create a fully connected network. Instead an exponential distribution is introduced

$$f(x;\lambda) = \begin{cases} \lambda e^{-\lambda x} & x \geq 0 \\ 0 & x < 0 \end{cases} \tag{4-1}$$

that determines the neuronal connections depending on the distance to each other with a mean value $\mu = 5$ and parameter $\lambda = \frac{1}{\mu}$. The distance between two neighboring neurons has the unit length 1 for the sake of simplicity.

Each neuron has exactly 28 outgoing synapses while no outgoing synapse goes to the same neuron multiple times which leads to the following connectivity plot - see Figure 4-2. A structure due to the probability distribution can be seen in the diagonal lines. Underlying reason is the transformation of a neuronal 2D array into a vector. Local proximity is approximately repeated by the width of the neuronal layer and correspondingly the structure fades with increasing distance. In Figure 4-2 each row shows the outgoing connections of one individual neuron and each synapse is assumed to have equal synaptic strength for simplicity reasons. Additionally, no transmission delays have been considered. If neuron j has a connection with

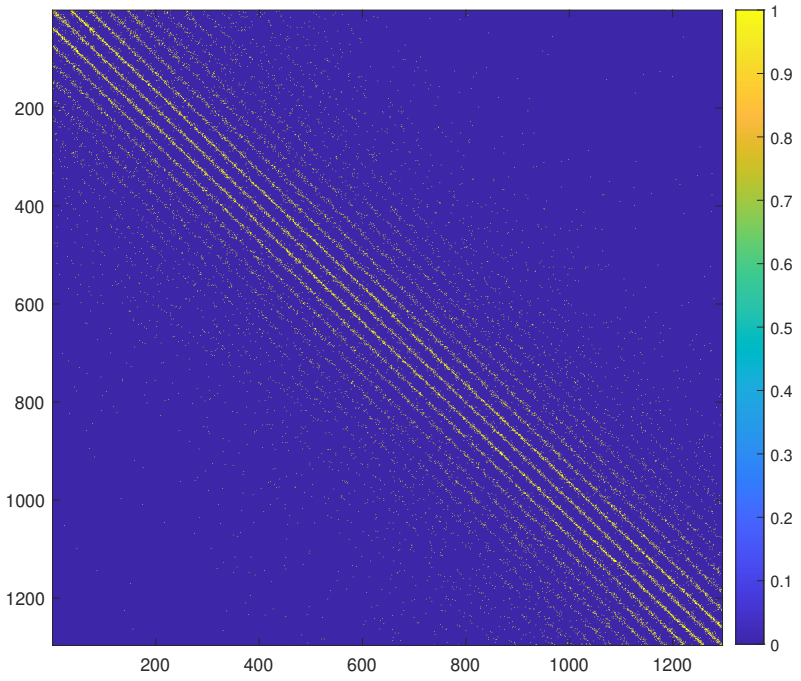

Figure 4-2: Neuronal Connections: The connectivity matrix according to a exponential distribution forms a wave like pattern. A dependency on spatial proximity is clearly visible by the fading colors on the off-diagonal parts. A connection between neurons is denoted with a 1.

neuron i the i^{th} element of row j is assigned the value of 1 and otherwise 0. In this way, the figure above can be interpreted.

In contrast to the random connections within the neuronal network, astrocytes show a much more structured network. In practice, astrocytes form gap junctions with neighboring astrocytes and overlapping of cells or links to further astrocytes are rare [22]. This has been realized in this network by linking each astrocytes to its directly neighboring cells resulting into minimal 2 and maximal 4 connections per astrocyte. The alternative ATP depending pathway of inter-astrocyte communication as described in Section 1-2-3 is neglected. Similar to the neuronal connections, Figure 4-3 shows the connectivity matrix of astrocytes and assigns a value of 1 to existing connections. Delay mechanism in the astrocytic gap junction are never mentioned most likely due to the in general slow astrocytic dynamics.

The neuronal and the astrocytic layer are connected by the astrocytic branches that envelop neuronal synapses. Since stimulation from neurons to astrocyte and from astrocytes to neurons exist and these relation is not exactly reciprocal, two connectivity matrices need be considered. From a spatial perspective, one astrocyte covers exactly r_{N-A} neurons - with r_{N-A} denoting the neuron-to-astrocyte ratio - and for simplification purposes it is assumed that the outgoing synapses from a neuron are spatially close enough to the astrocyte assigned to the presynaptic neuron. This denotes the connection scheme between presynaptic neu-

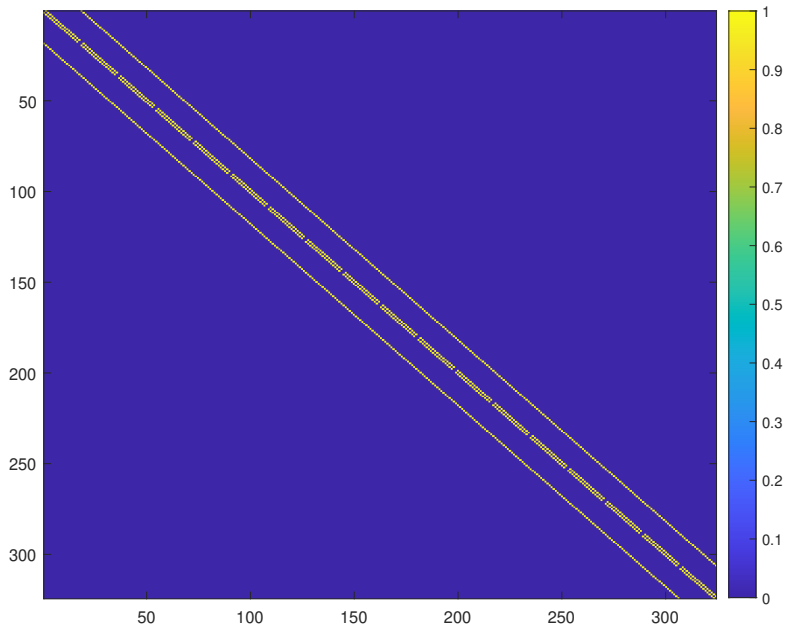

Figure 4-3: Astrocytic Connections: The connections within the astrocytic syncytium follow a clear pattern. Only directly neighboring cells form gap junctions. Hence, a clear pattern is visible in the connectivity matrix.

rons and astrocytes and means that the spiking neurons affect only the astrocyte in their direct surrounding. Figure 4-4a illustrates the spatial structure of the dual layer model with $r_{N-A} = 4$. Only neuronal and astrocytic cells are depicted without any connectivity for better visibility. Analog, to the figures above the connectivity matrix between the neuronal layer and the astrocytic layer is shown in 4-4b.

The connections between astrocytes and postsynaptic neurons are based on the neuronal connections but a slight adjustment is present according to the ration r_{N-A}. The following Figure 4-5 shows the connectivity matrix between astrocytes and postsynaptic neurons. It shows a more densely connected network compared to the connectivity matrix in Figure 4-4a. Naturally, the structure resembles the neuronal connectivity matrix with the fading oblique lines. An alternative connectivity scenario with astrocytes neighboring the postsynaptic neurons being affected by the action potential will be brought up as an additional simulation scenario in Section 4-3.

One important addition compared to [5] are inhibitory neurons. Releasing the neurotransmitter GABA instead of glutamate has a hyperpolarizing effect on the postsynaptic neuron and prevents neuronal activity. At the same point, inhibitory neurons are known to have an important role in synchronization of neuronal activity [57]. The strong inhibitory effect of gabaergic neurons calm the excitatory neurons in a uniform way. The synchronizing effect is obtained by simultaneous decay of the inhibitory neurotransmitters' effect. Following experimental data of mammalian cortices, the ratio between excitatory and inhibitory neurons

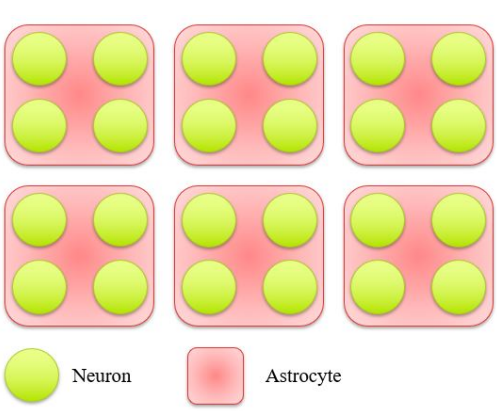

(a) Structure of the Dual Layers: A graphic for illustrating purposes shows the neurons as green round cells embedded in the astrocytic cells - depicted as red squares with round edges. The standard neuron-to-astrocyte ration r_{N-A} was selected for the graphic

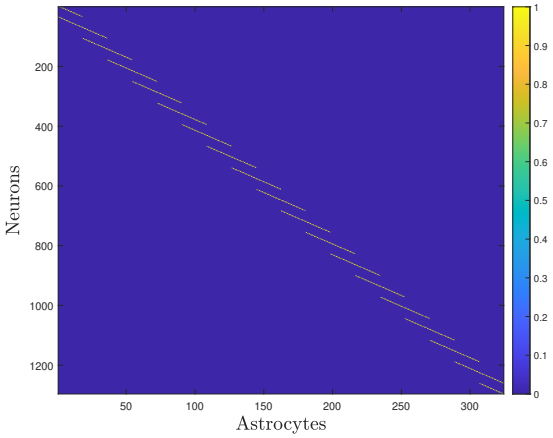

(b) Neuron-Astrocyte Connectivity: The connectivity matrix between neurons and astrocyte has a characteristic spatial structure. The cells of each layer having the same grid position are connected while taking the neuron-to-astrocyte ration r_{N-A} into account.

Figure 4-4: Overview of Standard Neuron-Astrocyte Connections

is $r_{E-I} = 4$ [45]. As the response mechanism of astrocytes to GABA release is not greatly explored at this point of time, the model neglects any influence of inhibitory neurons to astrocytes. At the same time astrocytes can induce slow inward current into inhibitory neurons as included in the standard mechanism. Astrocytes stay basically unaffected by the presence of inhibitory neurons except of their missing contribution for activating the glutamate induced IP_3 production J_{glu}. The distribution between inhibitory and excitatory neurons is randomized uniformly over the neuronal layer as depicted in the following figure 4-6.

The yellow squares represent excitatory neurons and the blue ones represent inhibitory neurons. Fittingly, the matrix for excitatory and inhibitory distribution is assigned with the respective values 1 and -1 for mathematical purposes.

The influence of inhibitory neurotransmission is modelled by a synaptic current I_{syn} consisting of an excitatory and an inhibitory part for each neuron as follows

$$I_{\text{syn}} = \sum_{k=1}^{N_{in,E}} \frac{\eta_{syn}\left(E_{\text{syn},E} - V\right)}{1 + \exp\left(\frac{-V_{\text{pre}}^{k}}{k_{\text{syn}}}\right)} + \sum_{k=1}^{N_{in,I}} \frac{\eta_{syn}\left(E_{\text{syn},I} - V\right)}{1 + \exp\left(\frac{-V_{\text{pre}}^{k}}{k_{\text{syn}}}\right)} \tag{4-2}$$

with two different synaptic reversal potential $E_{syn,E/I}$ to account for the different effects of inhibitory and excitatory neurotransmission. This equation for a divided synaptic current is taken from [58]. While there are many possibilities to assign different values to different classes of connections, the model features only one, uniform synaptic strength η_{syn} due to simplicity reasons.

Different aspects of the neuron-astrocyte network are shown above. To summarize the network model, the following table gives an overview of most of the important parameters. The

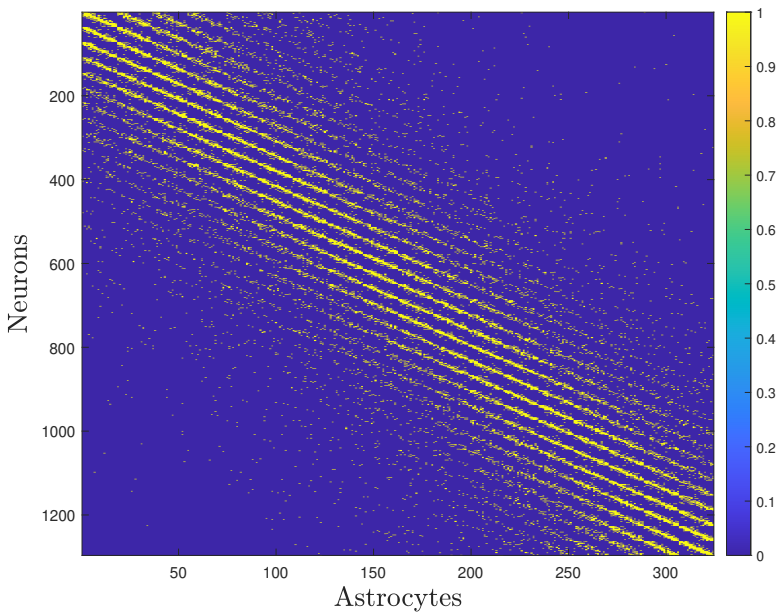

Figure 4-5: Astrocyte-Neuron Connectivity: The connectivity matrix between astrocytes and postsynaptic neurons is strongly associated to the neuron-to-neuron connections.

simulation model itself gives the freedom to change each parameters to a limit extent depending on how it affects linked parameters and feasibility for building the network.

N_E	Number of neurons	1296
N_A	Number of astrocytes	324
$N_{E,Syn}$	Number of outgoing synapses of a single neuron	28
λ	Rate of Exponential Distribution	5
$N_{A,Syn,min}$	Minimum number of outgoing gap junctions of a single astrocyte	2
$N_{A,Syn,max}$	Maximum number of outgoing gap junctions of a single astrocyte	4
r_{E-I}	Ratio of excitatory to inhibitory neurons	4

Table 4-1: Overview of Network Parameter

As already mentioned before, all parameter used in the mathematical analysis and the numerical simulation are also given in the Appendix A.

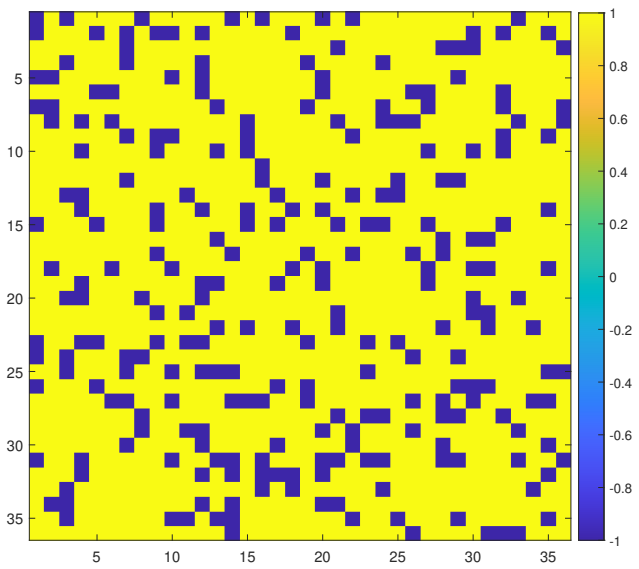

Figure 4-6: Distribution of Excitatory and Inhibitory Neurons: Excitatory neurons in yellow and inhibitory neurons in blue are distributed equally over the neuronal grid in accordance to the ratio r_{E-I}.

4-2 Simulation Protocol

As already mentioned before, the simulation protocol is inspired by classical experimental protocols such as [4]. In order to restrict the computation time, the total simulation time is limited to 6 seconds. A basic sequence of stimulation, delay period and recall is defined in accordance to classic working memory experiments. Generally, working memory experiments can be classified into single-item and multi-item trials referring to whether the test subject is required to keep one item or several items in working memory [5]. Consequently, the simulation protocols include both types of experiments. In total 5 different simulation protocols are created from which 2 result into persistent activity and 3 lead to sparse activity. The table below gives an overview of each protocol.

Simulation Protocol	Activity	Items	Recall
Protocol 1	Persistent	Single	No
Protocol 2	Sparse	Single	Specific
Protocol 3	Sparse	Single	Unspecific
Protocol 4	Sparse	Multiple	Specific
Protocol 5	Persistent	Multiple	Specific

Table 4-2: Overview of Simulation Protocols

Before the protocols are examined in more detail, a short overview of the different items or input signals is given in Figure 4-7. While other simulation scenarios used ciphers [5],

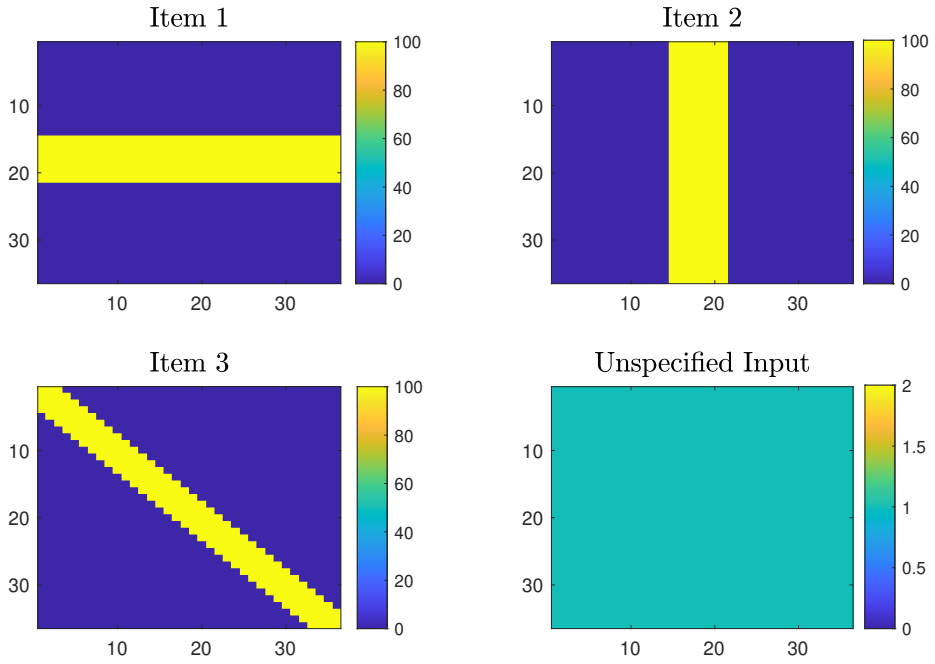

Figure 4-7: Overview of Input/Recall Signals: The three items which the neuron-astrocyte network is trained with and an additional uniform input for an unspecified input recall are shown. The depicted signals are ideal without any superimposed noise signals.

letters [58] or faces [59], the choice here is made towards more abstract items. Three lines with different orientations in accordance to the angular orientation in the experiments by [4] are the basis for stimulation.

The three items which are essentially implemented as input signals to the neuronal layer consist of a horizontal line, vertical line and a diagonal line. Additionally, an unspecified input signal is shown which is used in the Simulation Protocol 3 in order to demonstrate that a specific recall cue is not necessary for functioning recall. Besides the ideal input signal, noise is added to the simulation scenarios during the entire simulation time as a noisy current I_{noise} similar to [5]. According to experimental observations, Poisson pulse trains with a firing frequency $f_{noise} = 15Hz$ evoke random pulse-shaped input currents of length $t_{noise} = 30ms$ to individual neurons of amplitudes $A_{noise} \in [-10\mu A, 10\mu A]$. Figure 4-8 below shows input currents due to noise stimulating the neuronal layer summed up over the first 0.1 seconds of the simulation time.

A major difference between the stimulation phase and the recall phase with a recall cue is the current strength. The input signal has an input $I_{training} = 100\mu A$ in order to activate the astrocyte dynamics. Reason for this rather strong value is the short input time and the relatively slow glutamate dynamics which need to exceed a threshold value for the stimulation of astrocytes. The input strength during the recall phase is given by $I_{test} = 3.5\mu A$. Reason for this is the firing behavior of the Izhikevich model which means for this case that no firing is present if only the recall current is applied.

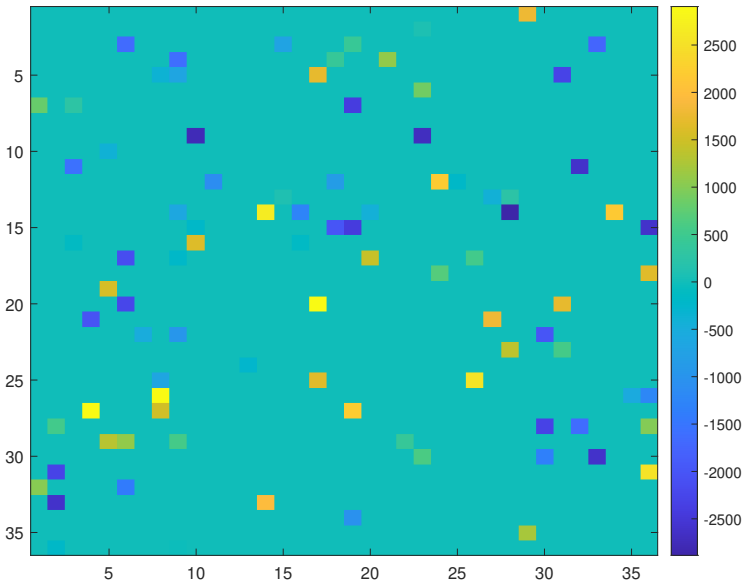

Figure 4-8: Background Noise: Noisy neuronal activity is realized via a Poisson spike train. The graphic depicts the input signals to neuron caused by this spike train summed up over an interval of $100ms$. This explains the high values in the color bar.

As summarized in Table 4-2, 5 simulation protocols are selected to test the neuron-astrocyte network model. In order to illustrate the mentioned experimental sequence the following Figure 4-9 is shown. More details for each simulation protocol is given together with its results in the corresponding subsection below.

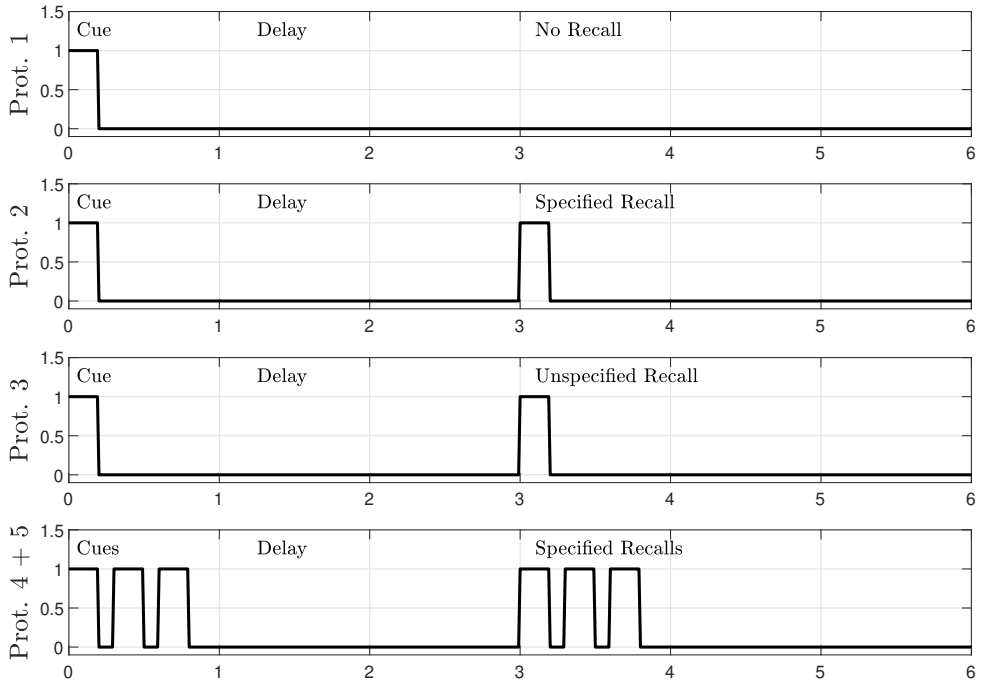

Figure 4-9: Overview of Simulation Protocols: The 5 simulation protocols as described in table 4-2 are depicted for illustration.

4-3 Simulation Results

In order to evaluate the working memory performance of the neuron-astrocyte network model, two key performance indicators (KPIs) are defined. In that way, different scenarios can be quantitatively compared. The underlying idea consists of separating the neuronal layer into two groups, namely the neurons who are excited by the ideal stimulus that represents the item (T) and the neurons who are not (NT). The KPIs C_1 and C_2 are introduced and their mathematical expressions as well as computational examples are given in Appendix C.

- C_1 ranges from 0 to 1 and takes the absence or presence of spiking into account without regard to firing frequency
- C_2 ranges from -1 to 1 and also considers the firing frequency of specific neurons to judge the WM performance

In the following, the different simulations results are shown and analyzed. Both plots of firing frequencies and KPI values give the possibility to compare the functionality of the working memory mechanism.

Protocol 1

The first simulation protocol reflects a single-item working memory task. During the first 0.2 seconds of the simulation, an input signal shaped as a horizontal line stimulates the neuronal layer - as it can be seen in the upper subplot of Figure 4-10. Within this simulation protocol, the tuning parameter is set to $\eta = 100\%$ which corresponds to strong astrocytic gliotransmission. Therefore, no additional recall cue is applied as persistent activity of the neurons encoding the input signal is expected. This phenomena of neuronal activity during

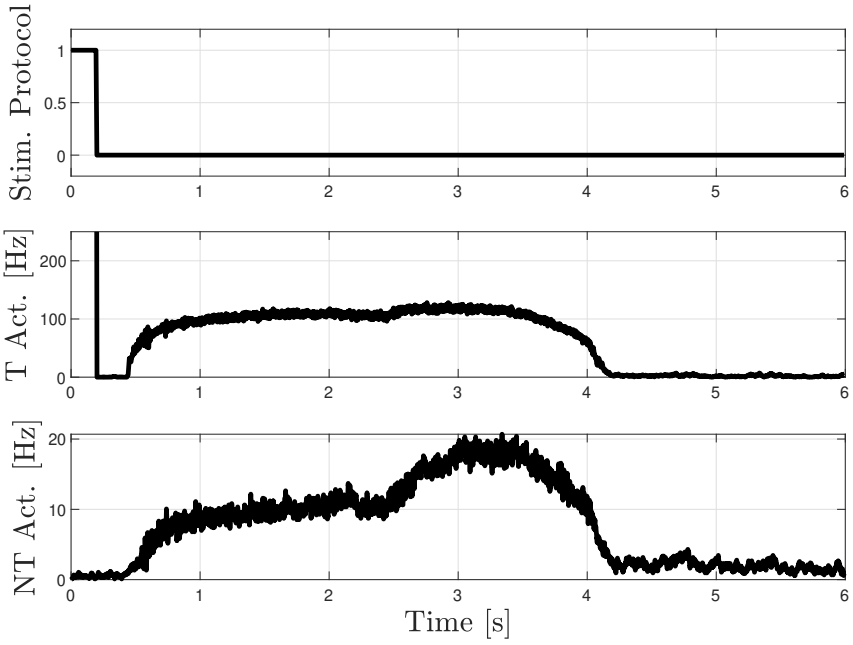

Figure 4-10: Simulation Results - Protocol 1: In the uppermost graph, the stimulation sequence - consisting of a single excitation in the beginning - is shown. Secondly the firing activity of target neurons (T) that reflect the stored item is given in contrast to the firing activity of non-target neurons (NT) below. It is clear that the single-item working memory task shows persistent activity for a limited time.

the delay period is clearly visible in the subplots 2 and 3 of Figure 4-10. While the firing frequency of non-target neurons is in the range of 5 to 20 Hz, target neurons show activity around 150 Hz over long period of time under the absence of any external stimulation. While the simulation results are quantitatively significantly larger than spiking behavior in experiments from [4] showed, the existence of persistent activity due to astrocytic feedback provides strong evidence of a possible astrocytic pathway for working memory.

Correspondingly the KPI values $C_1 = 0.8950$ and $C_2 = 0.2485$ show a decent WM performance - comparison can be drawn with Example 1 and 2 in Appendix C. Taking both the KPI values and the graph into account, the information is stored in working memory during the delay period.

Protocol 2

The second simulation protocol shows a single-item working memory task with reduced astrocytic gliotransmission leading to $\eta = 25\%$. After a short stimulation period of 0.2 seconds and an input-free delay phase of 2.8 seconds, here a short recall cue is applied to the neurons. The recall cue with $I_{test} = 3.5\mu A$ is a weak and noisy version of the original stimulation with $I_{train} = 100\mu A$. The superimposed, uniform noise signal has mean value $\mu_I = 0$ in the interval $[-1, 1]$. Looking at the graphs 2 and 3 of the Figure 4-11 shows a quasi-random spiking behavior of the non-target neurons with a average firing frequency of around 1.5 Hz and simultaneously a similar behavior for the target neurons except for the original stimulation and the recall period. Although the firing frequency of the target neurons during the recall phase is reduced compared to Protocol 2, the distinction between target and not-target neurons is very clear.

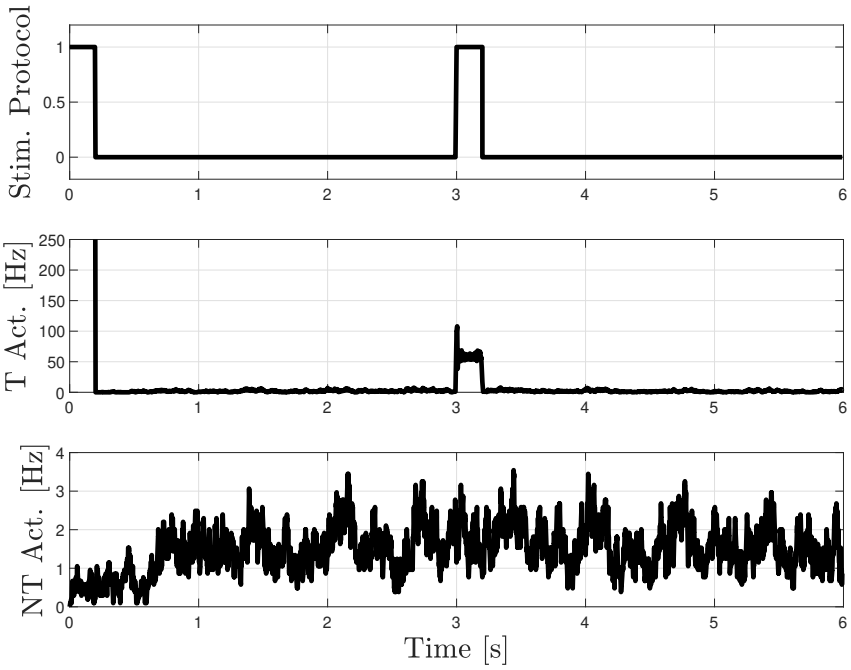

Figure 4-11: Simulation Results - Protocol 2: The single-item working memory task shows sparse activity except during the recall phase.

The above-mentioned differences to the first simulation results are only partially reflected within the KPI values of $C_1 = 0.7844$ and $C_2 = 0.8365$. While the C_1 value clearly decreased compared to Protocol 1, C_2 increased significantly. This observation is explained by the fact that KPI C_2 focuses on the distinction of the average firing frequency between target and non-target neurons which is enormous for Protocol 2. The drop of C_1 might be lead back to the general decrease of firing frequency which affects both the target and the non-target neurons but it still surprises. Nevertheless, both KPI values as well as Figure 4-11 indicate reasonable WM performance. Noteworthy, the average firing frequencies of both target and non-target during the delay period are equivalently small. Hence, the given scenario can

be classified as sparse neuronal activity giving evidence that astrocytic gliotransmission can provide a functional working memory model with both persistent and sparse activity during the delay period.

Protocol 3

So far, the recall cue resemble the original item only differing in the current strength and some overlying noise. In order to show a more robust performance an unspecified recall cue is applied in Protocol 3 while all the simulation sequence and other parameters equal Protocol 2. The unspecified recall cue affects all neurons equally and the recall period can therefore be more abstractly seen as a phase with increased attention. The tuning parameter is set to $\eta = 25\%$ and corresponds to sparse neuronal activity during the delay period. As it is

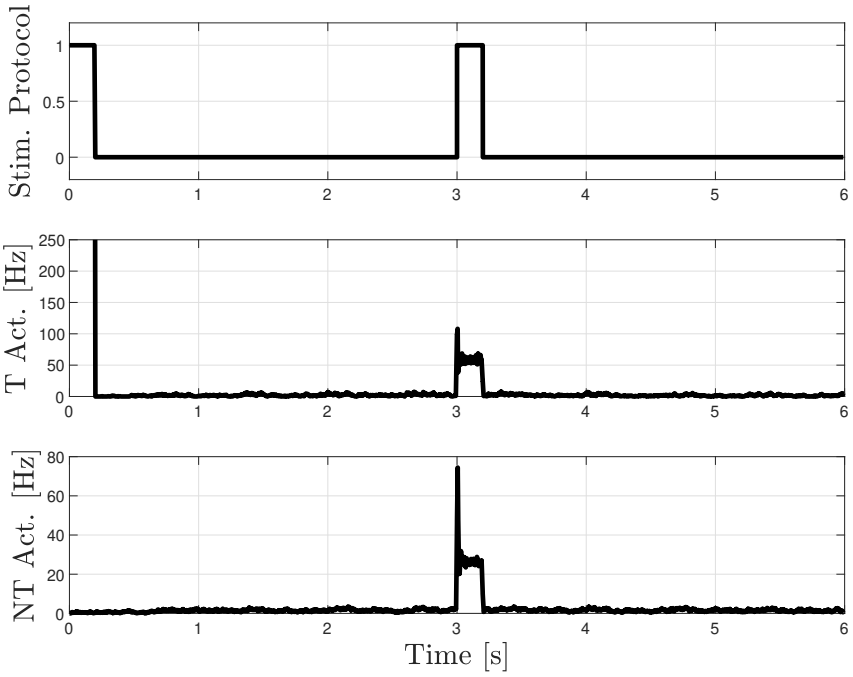

Figure 4-12: Simulation Results - Protocol 3: The single-item working memory task shows sparse activity except of the recall activity. An increase spiking behavior is visible for both target and non-target neurons.

visible in the second and third graph of Figure 4-12, both target and non-target neurons follow similar behavior and sparse activity throughout the time is interrupted by the recall cue causing enhanced activity for both neuronal groups. The average firing frequency for both groups shows a clear difference between the target - $f_T \approx 100$ - and non-target neurons - $f_{NT} \approx 30$. Although all neurons are stimulated by the same input current $I_{app} = 3.5\mu A$, the target neurons show significantly larger activity due to the additional astrocytic current I_{astro}.

The KPI values $C_1 = 0.6695$ and $C_2 = -0.2776$ give a reasonable feedback. Both C_1 and C_2 show worse performance than the previous simulation scenarios but the values are significantly better than for the randomly spiking network - as seen in Example 1 of Appendix C.

Reason for the C_2 decrease is the unspecified recall cue affecting all neurons as well as the fact that there are many more non-target neurons than target neurons which lead to a negative value. Despite the positive aspects found in Figure 4-12, it has to be said that Protocol 3 shows so far the worst working memory performance.

Protocol 4

Protocol 4 describes the first multi-item simulation scenario. Instead of only one input signal, three input signals are applied sequentially with short intermediate breaks. Similarly, the recall cue includes all three items with largely reduced strength and additional noise. A unspecified recall cue is not able to selectively trigger a stored item. Figure 4-7 displays all input signal including the second item consisting of a vertical line and the third item representing a diagonal line. The inputs are selected in a way to minimize the neurons that are excited multiple times. Analog to Protocol 2 and 3, weak gliotransmission ($\eta = 25\%$) is selected for this scenario. Figure 4-13 clearly shows sparse activity during the delay period in the subplot 2 and 3. All three recall cues triggers responses by strongly enhanced neuronal activity of the target neurons while non-target neurons show no significant increase.

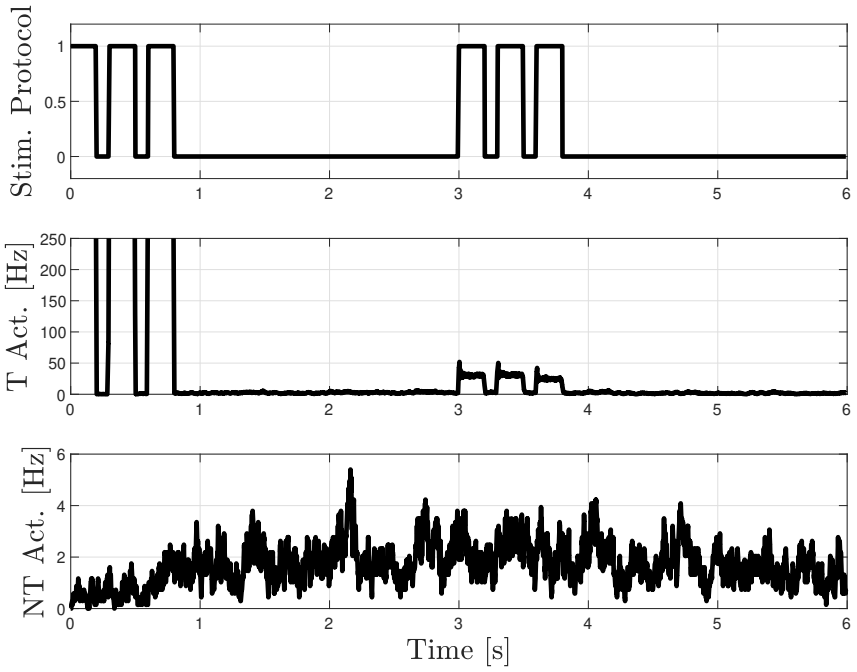

Figure 4-13: Simulation Results - Protocol 4: The multi-item working memory task shows sparse activity except of the recall phases.

Compared to the single-item scenario of Protocol 2 the KPI $C_1 = 0.8113$ and $C_2 = 0.8312$ show similar values indicating that a performance loss - due to the higher required memory capacity - is not present. There is even a slight improvement which we associate with the higher number of target neurons and the triple stimulation of a neuronal subset. In conclusion, the results show proper performance of the neuron-astrocyte network model for a

multiple-item working memory task.

Protocol 5

Analog to the single-item cases, the multi-item task is also simulated with strong gliotransmission - $\eta = 100\%$ - while the general simulation sequence is equal to Protocol 4. The application of recall cues - in contrast to Protocol 1 when no recall cue is applied - can be justified by the desire of evoking only specific items of the stored item pool. Naturally, this additional recall cue has to be kept in mind when examining the results.

Already during the stimulation period the influence of astrocytic feedback is visible as shown in the second graph of Figure 4-14. Similar to the single item scenarios, the overall firing frequencies for target and non-target neurons is enhanced compared to weak gliotransmission. The non-target neurons show an equal evolution compared to Protocol 1 - see Figure 4-10. During the recall phases, enhanced firing frequencies of the target neurons is clearly visible while the non-target neurons stay completely unaffected.

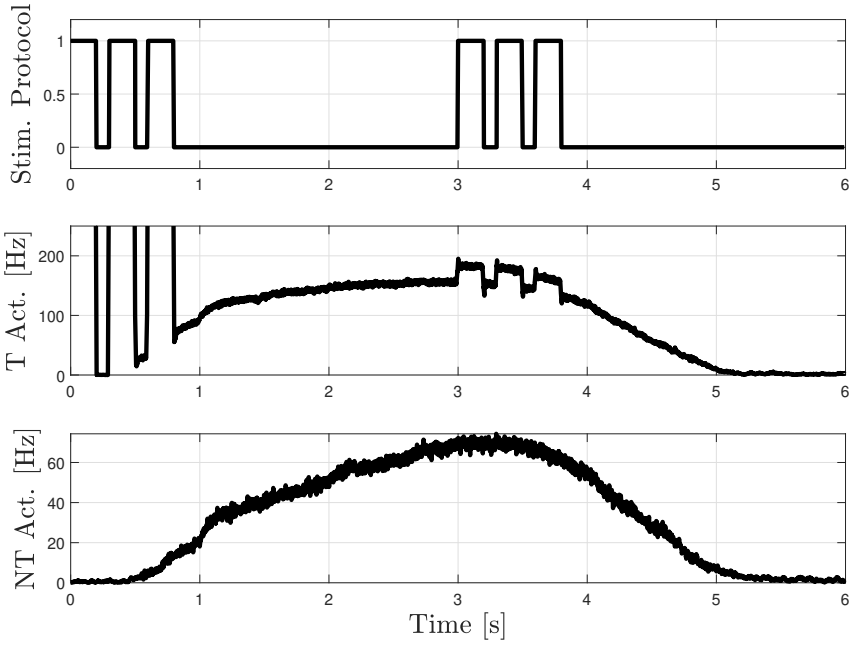

Figure 4-14: Simulation Results - Protocol 5: The multi-item working memory task shows persistent activity with additional elevations during the recall phases.

The KPI values $C_1 = 0.6650$ and $C_2 = 0.3945$ show a significant reduced memory performance compared to Protocol 4 which is connected to the overall higher excitation of non-target neuron due to higher astrocytic feedback. Especially, C_2 is affected by this overall increase of neuronal activity. Nevertheless, the simulation according to Protocol 5 shows good working memory performance.

No Gliotransmission

In order to exclude the possibility of other underlying mechanisms for the WM performance, in the following the absence of gliotransmission is investigated. Simulation Protocol 2 is reused with zero astrocytic gliotransmission ($\eta = 0$) and Figure 4-15 shows the results.

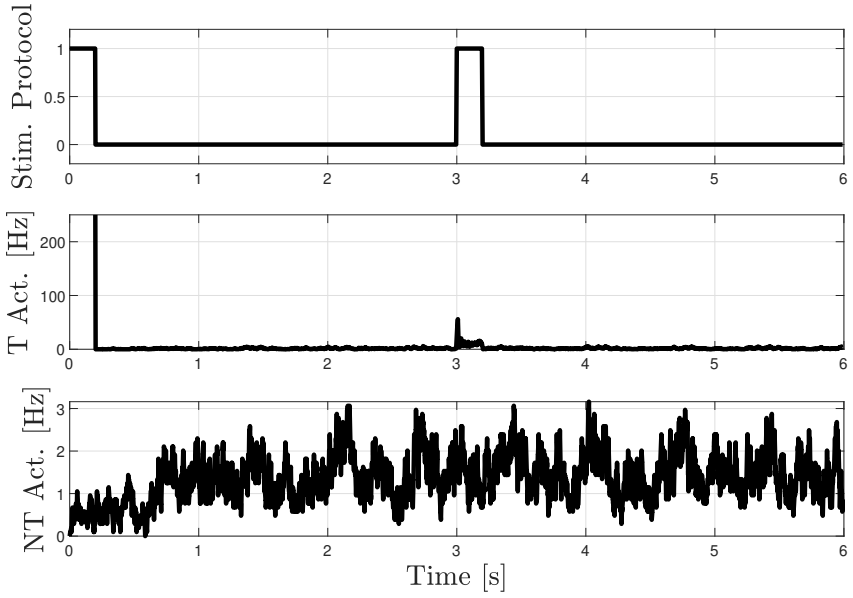

Figure 4-15: Simulation Results - No Gliotransmission: The single-item working memory task shows sparse activity overall time and no significant recall activity indicating poor memory performance.

Naturally, the third graph visualizing non-target behavior is very similar to the standard Protocol 2. In contrast, the second graph depicts a significant decrease in neuronal activity. The extremely slight plateau during the recall period can be explained by the noisy recall cue stimulating the target neurons. Correspondingly, the KPI values $C_1 = 0.5185$ and $C_2 = 0$ for the second protocol without gliotransmission indicate a large performance deficit. Especially, C_1 is very close to a completely randomly spiking network - compare with Example 1 in Appendix C - possibly due to the strong general decrease in neuronal activity. In conclusion, it can be stated that astrocytic gliotransmission is clearly the underlying mechanism for working memory function in this simulation scenario. To further examine the WM robustness of this neuron-astrocyte network, the number of astrocytes is reduced in the following while following Protocol 2 for all other parts.

Increased Neuron-Astrocyte Ratio

This simulation scenario focuses on the neuron-astrocyte ratio r_{N-A}. An increase of r_{N-A} translates to the spatial proximity of 9 neurons for one astrocyte instead of 4 neurons for one astrocyte. Originally, the number of astrocytes is $N_A = 324$ which is here reduced to less than half of it $N_A = 144$. All other parameters are equivalent to Protocol 2. Comparing

Figure 4-16 to the original results in Figure 4-11 shows no clearly visible changes although the number of astrocytes is reduced significantly. Examining the KPI values $C_1 = 0.8122$ and $C_2 = 0.8391$ shows even a slight improvement of memory performance compared to the original parameters. A possible reason for this development is the reduced effect of inhibitory neurons on astrocytes. In the original network, an astrocyte is linked to 4 neurons and referring to the unlikely but possible scenario of 2 neurons being inhibitory basically prevents the astrocytic calcium elevation.

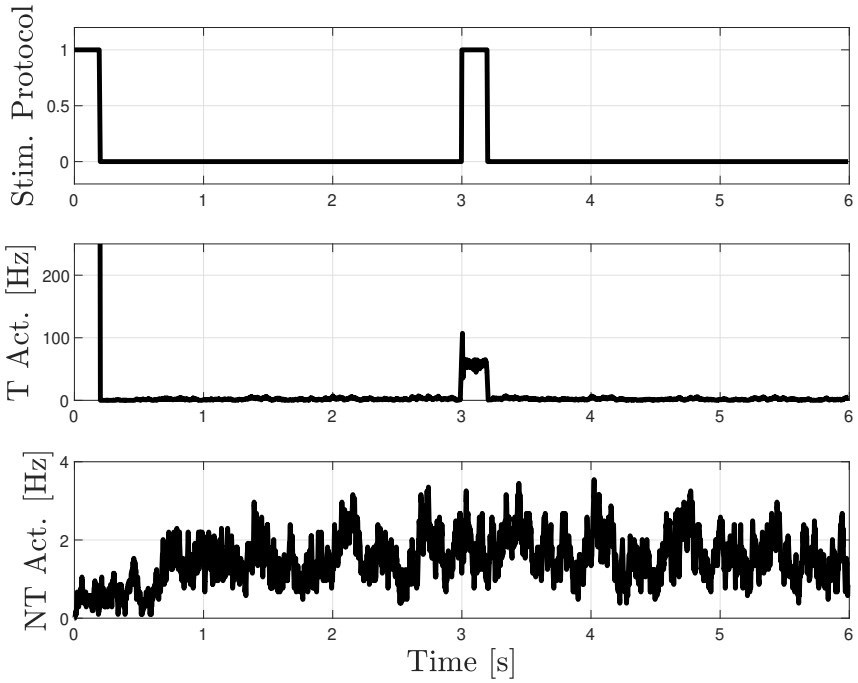

Figure 4-16: Simulation Results - High Neuron-Astrocyte Ratio: The single-item working memory task shows sparse activity except during the recall phase. No considerable difference to the original simulation results are visible.

The results of this scenario show the robustness of the network and its capability of functioning even for less memory-storing astrocytic units. There certainly exists a limiting astrocytic number $N_{A,lim}$ that effectively prevents the operability of the working memory task but it is not reached yet.

Alternative Neuron-Astrocyte Connectivity Matrix

As already mentioned in Section 4-2, it is assumed that the synapse is spatially close to the presynaptic neuron and therefore connected to the neighboring astrocyte. In reality, the synapse and therefore the astrocyte enwrapping it are more likely somewhere between the postsynaptic and presynaptic neuron. In the following, the simulation results are shown for Protocol 2 with alternative neuron-astrocyte connections that assume synaptic proximity to the postsynaptic neuron and therefore the astrocyte spatially close to the postsynaptic neuron is affected by the glutamate release. In principle, the other extreme is modelled in this

scenario. The condition for glutamate induced IP_3 production is adapted by assuming half of the incoming synapses have to exceed the glutamate concentration G_{thr}. All other simulation parameters are equal to Protocol 2. The simulation results are shown in Figure 4-17.

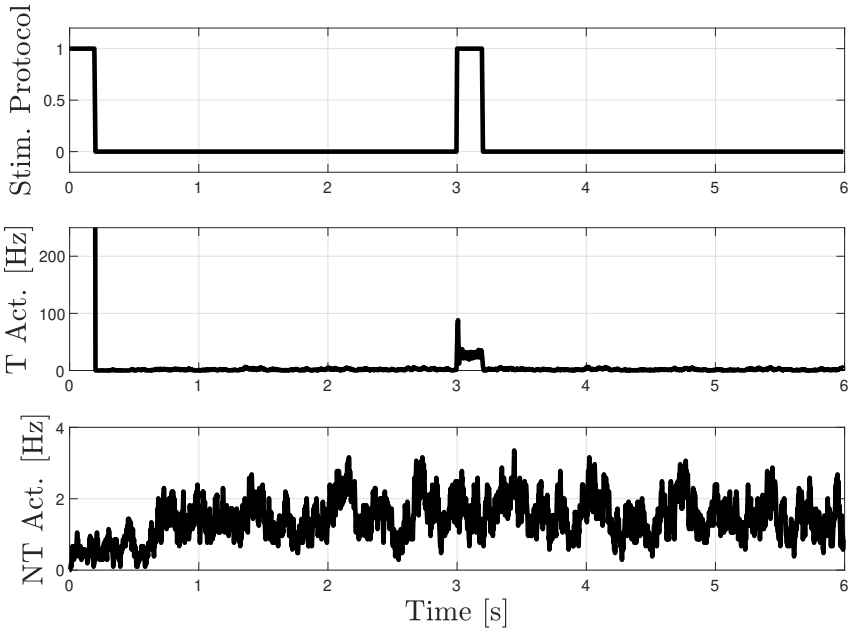

Figure 4-17: Simulation Results - Alternative Neuron-Astrocyte Connectivity: The single-item working memory task shows sparse activity throughout the delay period.

The overall neuronal activity increase is equal compared to the previous neuronal-astrocyte connectivity regarding the non-target neurons. On the other side, the target neurons are clearly excited during the recall phase but the firing frequency is reduced compared to the original simulation. The KPI values $C_1 = 0.6257$ and $C_2 = 0.6709$ support the analysis above. C_1 and C_2 are significantly lower than for the standard Protocol 2.

All in all, it can be stated that the alternative connectivity between neuronal and astrocytic layer reduces but not destroys the working memory performance. Reason is the spatial distribution of slow inward current that replaces a item-selective neuronal stimulation. Tuning specific parameter for this simulation scenario might increase the working memory performance.

4-4 Discussion

In the following, the numerical results obtained via network simulations are shown for each Protocol.

Protocol	**Activity**	**Items**	**Recall**	C_1	C_2
1	Persistent	Single	No	0.8950	0.2485
2	Sparse	Single	Specific	0.7844	0.8365
3	Sparse	Single	Unspecific	0.6695	-0.2776
4	Sparse	Multiple	Specific	0.8113	0.8312
5	Persistent	Multiple	Specific	0.6650	0.3945

Table 4-3: Overview of Simulation Results

In the previous section, the results of five different protocols all related to WM experiments are given. Simulation of Protocol 1 and 2 shows that astrocytic gliotransmission enables WM performance both in the presence and absence of neuronal firing within the delay period. This means that the information is not stored in neuronal activity but in astrocytic calcium elevation. Additionally, Figure 4-10 clearly shows a temporal limitation of 4 seconds after which the astrocytic excitation drops in the absence of further stimulation which is coherent with experimental data [4]. The functionality of the neuron-astrocyte network has even been proven for a black signal in Protocol 3. The stored information has been recalled after silent delay period with a uniform signal providing no information.

While "the magical number seven plus or minus two" [60] has not been reached with our multi-item simulation. an important feature of WM has been demonstrated by storing several pieces of information at once in our network. Three input signals have been successfully retrieved for weak as well as strong gliotransmission which follows the results of the single-item simulations. Hence, it has been shown that astrocytic gliotransmission via SIC towards the postsynaptic neuron provides a pathway for WM functionality. Simultaneously, experimental observation of varying neuronal activity can be reproduced by simple adjustment of gliotransmission efficacy η.

Chapter 5

Conclusions and Future Directions

In the previous chapters of this master thesis, the possibility of an astrocytic pathway for working memory has been discussed and a neuron-astrocyte network model has been introduced. Its components have been analyzed and the reasoning behind specific choices has been given. Furthermore, the analytical and numerical results for the tripartite synapse as well as simulations results of the complete network model in the context of working memory have been shown.

5-1 Conclusions

Looking at the results shown in the analysis of Section 3-3 and the simulation results of Section 4-3, the overall evidence points to a possible pathway of astrocytes for working memory tasks.

The analysis of the extended astrocyte dynamics has shown that different, locally stable equilibrium points show both sparse and persistently active postsynaptic behavior. For both weak and strong gliotransmission, astrocytic dynamics have been equivalent which indicates that sparse and persistent neuronal activity in this context has been merely a product of astrocytic feedback but do not affect the astrocytic dynamics. The contribution of a different gliotransmission formulation has enabled this variety of spiking behavior. Additionally, different equilibrium values for astrocytes - for the unperturbed and stimulated case - show the capability of astrocytes to respond to neuronal activity. It has to be stressed that all selected models for neurons, astrocytes and further dynamics have been taken from or derived from renowned literature - especially [5] - which promotes the meaningfulness of these results. Local stability analysis in combination with numerical simulation shows that the equilibrium states are indeed attracting steady-state values of the system within a biologically feasible region.

The results with regard to the tripartite synapse have been extended by investigating a network model that reflects a human or primal prefrontal cortex to an appropriate degree. Due

to the high number of mathematical equations, simulations have been executed to investigate the network performance. Connectivity features have been chosen to model the reality and assumptions for simplicity reasons have been mentioned. Different protocols for the network model consisting of 1296 neurons and 324 astrocytes as standard have been created to imitate classic experimental procedures. The network is able to handle working memory tasks with a single item for several scenarios showing sparse and persistent activity depending on the strength of gliotransmission which has not been done in existing literature. Simultaneously, the simulation has shown that the absence of astrocytic feedback causes the working memory performance to collapse completely. Thus, recurrent neuronal connections have not been sufficient in this network model to uphold the item in memory. In addition to the single item case, the neuron-astrocyte network has also been tested storing multiple items. The overall performance has shown similar quality compared to the single-item scenarios and also compared to reference literature - e.g. [5]. The items itself have purposely been kept general.

Lastly, the influence of one main assumption and one important parameter has been shown namely the connectivity between the neuronal and the astrocytic layer and the ratio of neurons-to-astrocytes r_{N-A}. These alternative scenarios provide insight in the robustness of the network model and its limitations. Especially, the spatial proximity of connections has played an important role as the selective stimulus of neurons is the fundamental principle of the memory functionality.

5-2 Future Research Directions

In Section 3-2, a tripartite model is simplified and analysed. The presented results of the stability analysis leaves room for further research. Currently, only local stability guarantee has been proven while no boundaries for the corresponding region of attraction has been set - at least regarding the model including state x_4^*. In this context, further research using Lyapunov-based methods might bring more light. Additionally, the time limitation of input signal as well as the capability of storing information only within a specific temporal limit have not been tackled by this approach. Simultaneously, further development of tools to analyse hybrid systems might help to directly investigate the system as described in Equation 2-2 without the need of simplification measures.

A more general research approach of the astrocytic influence on neuronal synchronization has already studied in the literature - see [61], [62] or [63]. Combining the idea of selective neuronal spiking describing specific input signals with the influence of neuronal synchronization might lead to interesting results. In order to perform a proper mathematical analysis, large simplification compared to the model used in this thesis must be applied. The astrocytic integrate and fire model by [39] could act as a starting point.

Focusing more on a biological perspective, several approaches can be made in order to improve the biological accuracy of the network. Most apparent is the missing link between inhibitory or GABAergic neurons and astrocytes. In this project, the presence of inhibitory neurons as important agents in the network is acknowledged but due to the lack of experimental research and evidence-supported models, the mechanism describing the effect of GABA on astrocytes is excluded. One important step for future research would be the examination of this pathway

as well as the corresponding astrocytic gliotransmitter release in order to bring more variety in this so far exclusive field of gliotransmission.

On top of that, specifically investigating the robustness of the memory performance of the given neuron-astrocyte network model could lead to insight in problems caused by neurological diseases. Simple examples include changing specific parameters like the synaptic strength η_{syn}, the astrocytic diffusion parameters d_{Ca} and d_{IP3} or the glutamate induced IP_3 production A_{glu}. Furthermore, reduced numbers of synapses or forced quiescence of neuronal or astrocytic cells can imitate specific cell death. There are certainly many more ways to test the performance robustness of the given network model.

Despite the thesis focus on astrocytes, general consensus withing researchers of this field says that mostly likely a combination of synaptic adaptation mechanism occurs simultaneously and creates a robust working memory pathway. In order to achieve a redundantly functioning and robust working memory system, these other pathways should be also included in the modelling approach and the simulation protocols. The most notable mechanisms are the synaptic facilitation and depression due to calcium and vesicle dynamics at the presynaptic terminal as well as the recurrent synaptic structures which are originally assumed to be the reason for the persistent spiking behavior.

Appendix A

Appendix I

Model Parameters

The following table shows the modelling parameter for the neuron model by Izhikevich [45] following [5].

Parameter	Description	Value
a	Time scale of the recovery variable u	0.1
b	Sensitivity of the recovery variable u	0.2
c	After-spike reset value of the membrane potential v	-65mV
d	After-spike reset of the recovery variable u	2
η_{syn}	Synaptic weight without astrocytic influence	0.025
$E_{syn,E}$	Synaptic reversal potential for excitatory synapses	0 mV
$E_{syn,I}$	Synaptic reversal potential for inhibitory synapses	-90 mV
k_{syn}	Slope of the synaptic activation function	0.2 mV

Table A-1: Overview of Neuronal Parameter

Besides the regular Izhikevich model an extension for the release dynamics for glutamate dynamics can be described with the following parameter [5].

Parameter	Description	Value
α_{glu}	Glutamate clearance constant	10 s^{-1}
k_{glu}	Efficacy of the glutamate release	600 μM s^{-1}

Table A-2: Overview of Glutamate Release Parameter

The following table shows the parameter for the astrocyte model by Li/Rinzel [48] with adaptions by [25] and [53].

Parameter	Description	Value
$\frac{1}{\tau_r}$	Rate constant for loss of IP3	0.14 s^{-1}
a_2	Ca^{2+} inhibition constant	0.14 $\mu M^{-1}s^{-1}$
c_0	Total calcium in terms of cytosolic volume	2.0 μM
c_1	Volume of ER over volue of cytosol	0.185
d_1	Dissociation constant for IP3	0.13 μM
d_2	Dissociation constant for calcium inhibition	1.049 μM
d_3	Receptor dissociation constant for IP3	943.4 nM
d_5	Calcium activation constant	82 nM
d_{Ca}	Calcium diffusion rate	0.05 s^{-1}
d_{IP3}	IP3 diffusion rate	0.1 s^{-1}
IP_3^*	Steady state concentration of IP3	0.16 μM
k_1	Rate constant of calcium extrusion	0.5 s^{-1}
k_2	Half-saturation constant for agonist-dependent calcium entry	1 μM
k_3	Activation constant for ATP calcium pump	0.1 μM
k_4	Dissociation constant for calcium stimulation of IP3	1.1 μM
v_1	Maximum calcium channel flux	6 s^{-1}
v_2	Calcium leak flux constant	0.11 s^{-1}
v_3	Maximum calcium uptake	2.2 μM s^{-1}
v_4	Maximum rate of IP3 production	0.3 μM s^{-1}
v_6	Maximum rate of activation-dependent calcium influx	0.2 μM s^{-1}
α		0.8

Table A-3: Overview of Astrocytic Parameter

The following table shows the parameter of the standard neuron-astrocyte network.

Parameter	Description	Value
N_E	Number of neurons	1296
N_A	Number of astrocytes	324
$N_{E,Syn}$	Number of outgoing synapses of a single neuron	28
λ	Rate of Exponential Distribution	5
$N_{A,Syn,min}$	Minimum number of outgoing gap junctions of a single astrocyte	2
$N_{A,Syn,max}$	Maximum number of outgoing gap junctions of a single astrocyte	4
r_{E-I}	Ratio of excitatory to inhibitory neurons	4

Table A-4: Overview of Network Parameter

Appendix B

Appendix II

Overview of Simulation Environments

Simulating biological neural network is a well-practiced manner of investigating specific neural behavior. There are several freely available software packages that provide a simulation environment for neuronal networks [64]. Within the research assignment of this master thesis, a number of those existing simulation environments including NEURON and BRIAN 2 have been examined regarding their usability for this project.

NEURON is the most popular neuronal simulation environment judging purely on the number of citations on Google Scholar of NEURON literature such as [65] or [66]. Developed at Yale University, the goal is to provide an user-friendly environment that enables simulation of individual neurons and neuronal networks with different ion channel dynamics - comparable to the Hodgkin and Huxley model - in order to bring experimental and computational scientist together. The simulation environment can be used via its graphical user interface and as a python package. The underlying code is written in the programming language hoc which enables fast computation time that is especially relevant for complex neuronal structures as well as large neuronal network sizes. NEURON allows the detailed modelling of spatial neuronal structures and is an important tool for researcher that examine the spiking behavior of individual neurons. Furthermore, accurate modelling of synaptic connections between neurons is possible. A great advantage is the large amount of online documentation and the active community that enables beginners a quick start. On the other side, the sole standard component of networks is the neuron and astrocyte dynamics have to be included as new models inside the environment. Consequently, the connection between neuron and astrocyte as well as astrocyt-to-astrocyte are not included in the standard NEURON package. In [67] a detailed single astrocyte has been modelled using the NEURON environment with extension of the cell dynamics by the author.

A second simulation environment with a large amount of users is Brian 2. In contrast to NEURON, this simulation environment focuses on neuronal networks rather than single neurons and the usage of manually written differential equations to define the single cell dynamics

replaces predefined functions. As a consequence, Brian 2 requires a lot more coding effort and coding accuracy and offers in return more flexibility and freedom for the user. Brian 2 is commonly used as a Phython package and sufficient material for beginners is available for a quick start. Similar to NEURON, the integration of astrocytes is not a standard feature of the environment but defining the cell dynamics itself is not a problem. More effort has to be taken when connecting the astrocytes with each other as well as connecting them with the neuronal network as synapses are defined by existing functions. In [21] the code for the simulation of a neuron-astrocyte network model using Brian 2 has been published and explained but it has to be said that compromises have been made in order to fit the frame of the environment.

Besides the two above-mentioned simulation environments, several others including GENESIS and NEST have been examined although partly to a smaller extent [64]. Due to the difficulties concerning the integration of astrocytes, the choice has been made to create an application-suited simulation environment outside of the existing ones in order to guarantee the flexibility and functionality of the neuron-astrocyte network that is required for the success of this project. Due to the author's personal affinity, Matlab is chosen over Python as the underlying program. Once the model dynamics have been chosen - as described in 3-3 - two main decision have to be taken. Firstly, the algorithm for the numerical integration has to be selected. Secondly, the time step Δt for the numerical integration needs to be defined. The usage of an algorithm with variable step size is possible but due to the time invariant dynamics, the higher complexity of those algorithms and the additional computation time for the step size, a constant time step is preferred for this case.

Matlab offers a variety of build-in solution for numerical integration such as the Matlab ODE Suite. Unfortunately, the ode-functions are not able to handle the hybrid dynamics of the given system. Event-functions give the possibility for simple state transitions which is sufficient for the classic jumping ball example. Nevertheless, it is not suitable for the complex dynamics depicted in Equation 2-2. Similarly, the Hybrid Equation Toolbox offers a build-in solver for hybrid equations but the handling of a network model has been proven to be not feasible. Consequently, the numerical integration will also be coded bottom up. In the following, this process is shortly examined.

Selection of Algorithm

Different numerical integration method exist to approximate differential equation for the classic initial value problem [68]. The most simple and classic numerical integration method is given by the Euler-Forward (EF) mechanism which is based on the linearization of the nonlinear dynamics $\dot{x} = f(x)$ as shown below:

$$\begin{aligned} f(x(t)) &= \lim_{\Delta t \to 0} \frac{x(t+\Delta t)-x(t)}{t+\Delta t-t} \\ &\Updownarrow \\ f(x(t)) &\approx \frac{x(t+\Delta t)-x(t)}{t+\Delta t-t} \\ &\Updownarrow \\ x(t+\Delta t) &\approx x(t) + \Delta t f(x(t)) \end{aligned} \tag{B-1}$$

Using the current state x^i, a step direction $df(x^i)$ can be computed and a small state update is executed before repeating this process again. Experience with numerical simulation has

shown that good performance of the Euler method requires small step sizes leading to high computation time. Runge introduced a generalization of the Euler method by taken more than just one time step into account. The classic Runge-Kutta method or RK4 algorithm uses 4 previous state values in order to reduce the step size while upholding the accuracy of the results. The update equation is defined as

$$x(t+\Delta t) = x(t) + \frac{1}{6}\left(k_1 + 2k_2 + 2k_3 + k_4\right)\Delta t \tag{B-2}$$

with the k_i values being defined in the following way

$$\begin{aligned} k_1 &= f\left(t, x(t)\right) \\ k_2 &= f\left(t + \tfrac{\Delta t}{2}, x(t) + \Delta t \tfrac{k_1}{2}\right) \\ k_3 &= f\left(t + \tfrac{\Delta t}{2}, x(t) + \Delta t \tfrac{k_2}{2}\right) \\ k_4 &= f\left(t + \Delta t, x(t) + \Delta t k_3\right) \end{aligned} \tag{B-3}$$

Implicit algorithms have not been considered due to the high nonlinearities of dynamics and the fact that no explicit solution has been found. In order to evaluate each numerical algorithm, simulation with both methods are executed and the results compared. The astrocyte dynamics have been selected as the base for comparison due to their stronger nonlinearities.

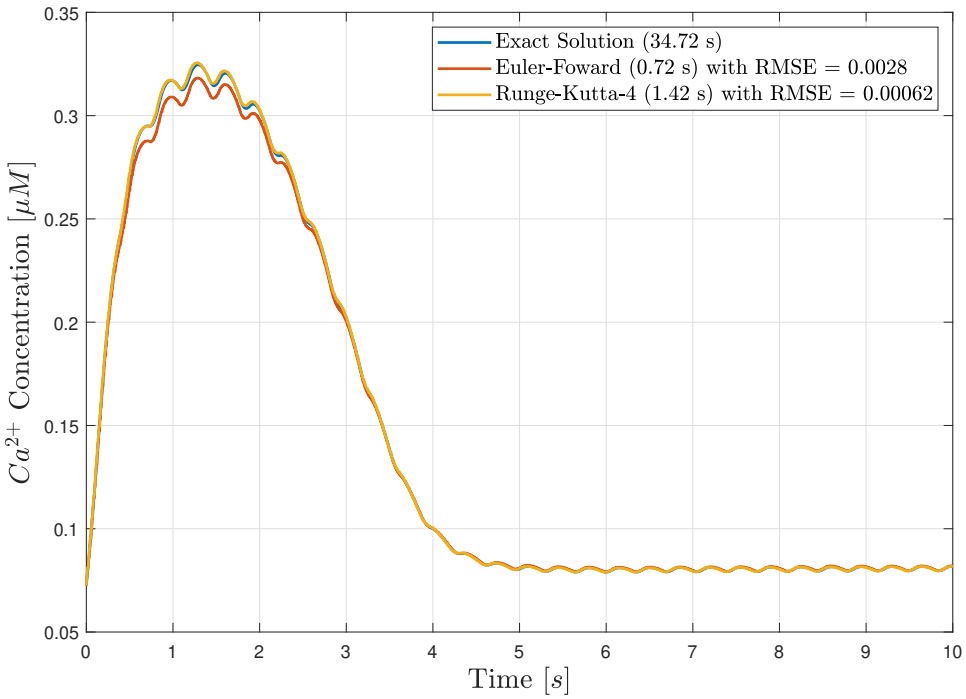

Figure B-1: Comparison of Solvers: The accuracy of the Euler-Forward solver and the Runge-Kutta-4 algorithm is compared to an "exact" solution using the same step size. The "exact" solution is derived via the Euler-Forward algorithm with a very small step size $\Delta t = 0.01ms$. The performance of the Runge-Kutta-4 solver is significantly better than Euler-Forward.

Figure B-1 shows the simulation accuracy of the Euler-Forward algorithm and the RK4 algorithm compared to an exact solution. For the same step size, there is a significantly larger root mean square error (RMSE) of the EF method. Although the computation time is approximately twice as high for RK4, further simulation have shown that the EF algorithm requires an eighth of the time step and four times the computation time to perform similar to RK4 which leads to the choice towards the RK4 algorithm. The "exact solution" that is depicted in the plot is actually derived by EF with an extremely small time step of $\Delta t_{exact} = 0.1ms$ in order to approximate the exact solution.

Secondly, the fixed time step for the neuron-astrocyte network model has to be selected. A compromise between high accuracy due to small time steps and high computational speed equivalent to large time steps is crucial. Due to the much faster neuronal dynamics, the Izhikevich model is used to define an appropriate value for Δt. The model itself is defined in Section 2-1-1 with an input signal $I_{app} = 5\mu A$ which leads to neuronal firing but allows a certain amount of visibility within Figure B-2.

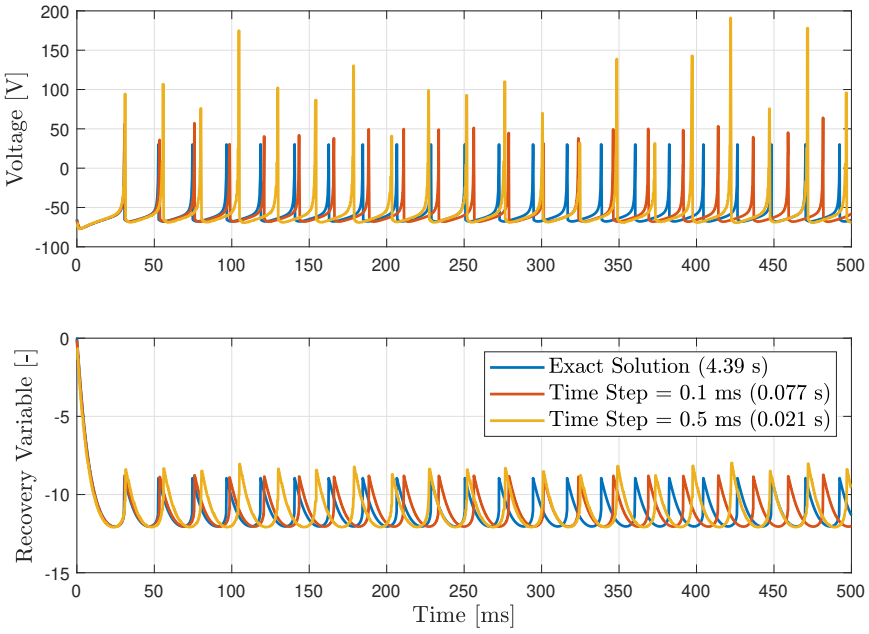

Figure B-2: Comparison of Time Steps: Using the Runge-Kutta-4 solver, three different time steps are compared. The "exact" solution with 0.001ms, the regular time step $\Delta t_1 = 0.1ms$ and a larger time step $\Delta t_2 = 0.5ms$. Especially the membrane voltage supports the usage of Δt_1.

Most commonly, a simulation time step $\Delta t = 0.1s$ is given in existing papers [5], [45]. This value has been selected as a starting point and possible higher values have been tested for reduction of computation time. Figure B-2 shows that an increase in Δt results into lagging dynamics compared to the exact solution. Using a time step $\Delta t = 0.5ms$ leads to 4 missed AP compared to 44 AP over $t_{sim} = 1s$ by the exact solution which is not acceptable in our case. Consequently, the simulation time step $\Delta t = 0.1ms$ is used throughout the simulation of the neuron-astrocyte network model. The "exact" solution is again computed by the EF

method using a extremely small time step $\Delta t_{exact,2} = 0.001ms$. The algorithm used for numerical integration with $\Delta t = 0.1ms$ and $\Delta t = 0.5ms$ is the RK4 method. This concludes the possible choices for the numerical integration.

In order to give an overview of the code that is used to run the simulation of the given neuron-astrocyte network model, the pseudo-code is depicted below. Naturally, the simulation code is divided into smaller function which are sequentially called from the *main* file. At the start of the simulation, the user can select between different simulation scenario - also called simulation protocols - which will be explained in the following section 4-3. Additionally, it is possible for the user to adjust some parameters if desired in the *parameter* file. In general, the parameters are simply loaded in the work space. Next, the neuron-astrocyte network model will be created meaning vectors for states and matrices for connectivity between the cells will be defined. Additionally, the initial states will be assigned respectively which correspond in this case to the unperturbed equilibrium states. Further on, the input signals will be defined according to the selected simulation protocol. Now the main part of the simulation begins. Within a for loop, the state update via the RK4 algorithm - separately for the neuronal layer and the astrocytic layer - is followed by the computation of the neuronal and astrocytic input for the following step. Following the simulation, key performance indicator are calculated and plots are created. Lastly, the existing data of input signal, neuronal voltage and calcium concentration will be reshaped and a video showing the neuronal firing and the astrocytic calcium concentration is generated which can be played if desired. The structure of the code is developed having the code of [5] available which has provided a proper starting point.

```
%% Pseudo Code: Structure of Main
Select_Simulation_Protocol
Initialize_N-A-Network
    load('parameters')
    create('vectors')
    create('connections')
    create('input_signals')
Run_Simulation
    For(Simulation_Time)
        Compute_Input_Signals
        State_Update_Neuron
        State_Update_Astrocyte
        Save_Necessary_Data
    End
Compute_KPI
Create_Plots
Create_Video
Play_Video
```

The detailed code is available in a folder besides the thesis report.

Appendix C

Appendix III

Key Performance Indicator

In the following this two groups of neurons will be referred to as target neurons P and non-target neurons $\bar{P}$ of the entire neuronal set N.

$$P \coloneqq \{\, N \mid \mathrm{I_{app}}(t = t_{stim}) \geq 1 \,\}$$

with t_{stim} having different values depending on a single-item or multiple-item case. The main principle is now to assign positive values for spiking target neurons and non-spiking non-target neurons during the recall period [5]. In order to give a good picture, two key performance indicators (KPIs) will be calculated. The first KPI will only consider whether a neuron has had an AP during a time interval $w = 10ms$ in the recall period. This spike detector value $M_{1,i}$ can be mathematically described using the indicator function I that assigns the value one to every element that fulfills its condition and zero otherwise.

$$M_{1,i}(t) = I\left[\left(\sum_{k=t-w}^{t} I\left[V_i(k) > V_{thr}\right]\right) > 0\right] \tag{C-1}$$

The time t for the evaluation will be selected as the middle of the recall period. Each neuron is assigned to a $M_{1,i}$ value which provides the basis for the following weighting process.

$$C_1(t) = \frac{1}{2}\left(\frac{1}{|P|}\sum_{(i)\in P} M_{1,i}(t) + \frac{1}{|\bar{P}|}\sum_{(i)\in \bar{P}} (1 - M_{1,i}(t))\right) \tag{C-2}$$

with the KPI $C_1(t) \in [0, 1]$ giving an evaluation of the working memory performance of the neuron-astrocyte network. The equation above takes both inactivity of target neurons as well as activity of non-target neuron negatively into account and is therefore a proper KPI. At the same time, the amount of firing of the neurons is not considered and noisy input has a significant influence on the KPI.

The second KPI takes also the number of spikes that occur during the time interval into account. In that manner, usually weak spiking due to signal noise has a reduced influence and the performance evaluation is more robust and meaningful. The spike count $M_{2,i}$ is defined similarly to the spike detection above.

$$M_{2,i}(t) = \left(\sum_{k=t-w}^{t} I\left[V_i(k) > V_{thr}\right] \right) \tag{C-3}$$

A vector containing the number of spiking during $w = 10ms$ for each neuron and similar to the first KPI an evaluation value is computed by weighting spiking target neurons and non-spiking target neurons.

$$C_2(t) = \frac{1}{S_{P+|\bar{P}|}} \left(\sum_{(i)\in P} M_i(t) - \sum_{(i)\in \bar{P}} M_i(t) \right) \tag{C-4}$$

with $S_{P+|\bar{P}|} = \sum_{(i)} M_i(t)$ denoting the total number of registered spikes. The interval for the second KPI value C_2 is within $[-1, 1]$. A disadvantage of the second KPI is that during minimal activity high performance values can occur although the main signal is more or less completely lost. This means that a combination of both KPI values should be used in order to give an appropriate judgement of the performance.

Example 1 - Random Spiking

A short example with a completely random spiking network showing uniform distribution of spiking probability should demonstrate the idea and lie a base line for the KPI values of the simulation scenarios. The average firing frequency during the recall phase is assumed to be $f_{recall} = 10Hz$. Analog to the simulation protocols, the total number of target neurons is $N_{E,T} = 252$ and consequently $N_{E,NT} = 1044$ non-target neurons. This gives the following KPI values for a completely dysfunctional working memory process.

The expectation of M_1 is given by $\bar{M_1}$ and is equal for each neuron.

$$\bar{M_1} = 0.1 \tag{C-5}$$

This leads to the following first KPI value.

$$\bar{C_1} = \frac{1}{2}\left(\frac{1}{252} 25.2 + \frac{1}{1044} 939.6 \right) = 0.5 \tag{C-6}$$

The expectation of M_2 is given by $\bar{M_2}$ and is equal to $\bar{M_1}$ due to the choice of firing frequency.

$$\bar{M_2} = 0.1 \tag{C-7}$$

Consequently, this leads to the following KPI value.

$$\bar{C_2} = 1/129.6\,(25.2 - 104.4) = -0.6111 \tag{C-8}$$

The KPI value $\bar{C_1} = 0.5$ and $\bar{C_2} = -0.6111$ denote the expected values for an impaired working memory model. Correspondingly, the expected KPI values for the different simulation

protocols should be significantly higher. The negative value of $\bar{C}_2$ can easily be explained by the fact that the number of non-target neurons is higher than target neurons while their firing frequency is equal.

Example 2 - Ideal Spiking

A second example for a perfectly well functioning working memory system gives a upper limit for the KPI values. Only the stimulated neurons are spiking during the recall phase with an uniform and precise firing frequency of $f_{recall} = 100Hz$. The numbers of target neurons $N_{E,T} = 252$ and non-target neurons $N_{E,NT} = 1044$ are taken as before. This leads to the following KPI values.

Again the expected value of M_1 is calculated but it can be classified in two groups for this case.

$$\bar{M}_{1,T} = 1 \quad \bar{M}_{1,NT} = 0 \tag{C-9}$$

This leads to the following KPI value C_1.

$$\bar{C}_1 = \frac{1}{2}\left(\frac{1}{252}252 + \frac{1}{1044}1044\right) = 1 \tag{C-10}$$

And correspondingly for M_2

$$\bar{M}_{2,T} = 1 \quad \bar{M}_{2,NT} = 0 \tag{C-11}$$

which is used to calculate C_2

$$\bar{C}_2 = 1/252\,(252 - 0) = 1 \tag{C-12}$$

For the ideal case, the KPI values amount to $\bar{C}_1 = 1$ and $\bar{C}_2 = 1$. These are the upper values of possible working memory performance. Clearly, they are in practice never achievable, and we expected values somewhere between Example 1 and Example 2 for our realistic network simulation.

Bibliography

[1] R. C. Atkinson and R. M. Shiffrin, "Human memory: A proposed system and its control processes," in *Psychology of learning and motivation*, vol. 2, pp. 89–195, Elsevier, 1968.

[2] C. Agulhon, J. Petravicz, A. B. McMullen, E. J. Sweger, S. K. Minton, S. R. Taves, K. B. Casper, T. A. Fiacco, and K. D. McCarthy, "What is the role of astrocyte calcium in neurophysiology?," *Neuron*, vol. 59, no. 6, pp. 932–946, 2008.

[3] G. Perea, M. Navarrete, and A. Araque, "Tripartite synapses: astrocytes process and control synaptic information," *Trends in neurosciences*, vol. 32, no. 8, pp. 421–431, 2009.

[4] S. Funahashi, C. J. Bruce, and P. S. Goldman-Rakic, "Mnemonic coding of visual space in the monkey's dorsolateral prefrontal cortex," *Journal of neurophysiology*, vol. 61, no. 2, pp. 331–349, 1989.

[5] S. Y. Gordleeva, Y. A. Tsybina, M. I. Krivonosov, M. V. Ivanchenko, A. A. Zaikin, V. B. Kazantsev, and A. N. Gorban, "Modelling working memory in spiking neuron network accompanied by astrocytes," *Frontiers in Cellular Neuroscience*, vol. 15, p. 86, 2021.

[6] N. Chowdhary, C. Barbui, K. J. Anstey, M. Kivipelto, M. Barbera, R. Peters, L. Zheng, J. Kulmala, R. Stephen, C. P. Ferri, *et al.*, "Reducing the risk of cognitive decline and dementia: Who recommendations," *Frontiers in neurology*, vol. 12, p. 765584, 2022.

[7] M. Prince, A. Comas-Herrera, M. Knapp, M. Guerchet, and M. Karagiannidou, "World alzheimer report 2016: improving healthcare for people living with dementia: coverage, quality and costs now and in the future," 2016.

[8] A. Lee and R. M. Gilbert, "Epidemiology of parkinson disease," *Neurologic clinics*, vol. 34, no. 4, pp. 955–965, 2016.

[9] A. Géron, *Hands-on machine learning with Scikit-Learn, Keras, and TensorFlow: Concepts, tools, and techniques to build intelligent systems.* O'Reilly Media, 2019.

[10] Q. Rao and J. Frtunikj, "Deep learning for self-driving cars: Chances and challenges," in *Proceedings of the 1st International Workshop on Software Engineering for AI in Autonomous Systems*, pp. 35–38, 2018.

[11] A. B. Porto-Pazos, N. Veiguela, P. Mesejo, M. Navarrete, A. Alvarellos, O. Ibáñez, A. Pazos, and A. Araque, "Artificial astrocytes improve neural network performance," *PloS one*, vol. 6, no. 4, p. e19109, 2011.

[12] E. R. Kandel, Y. Dudai, and M. R. Mayford, "The molecular and systems biology of memory," *Cell*, vol. 157, no. 1, pp. 163–186, 2014.

[13] A. D. Baddeley and G. Hitch, "Working memory," in *Psychology of learning and motivation*, vol. 8, pp. 47–89, Elsevier, 1974.

[14] P. S. Goldman-Rakic, "Cellular basis of working memory," *Neuron*, vol. 14, no. 3, pp. 477–485, 1995.

[15] S. Funahashi, "Prefrontal cortex and working memory processes," *Neuroscience*, vol. 139, no. 1, pp. 251–261, 2006.

[16] W. Gerstner, W. M. Kistler, R. Naud, and L. Paninski, *Neuronal dynamics: From single neurons to networks and models of cognition*. Cambridge University Press, 2014.

[17] M. A. Clark, J. Choi, and M. Douglas, "The nervous system," *Biology 2e*, 2018.

[18] W. A. Catterall, "Structure and function of voltage-gated ion channels," *Annual review of biochemistry*, vol. 64, no. 1, pp. 493–531, 1995.

[19] A. Verkhratsky and M. Nedergaard, "Physiology of astroglia," *Physiological reviews*, vol. 98, no. 1, pp. 239–389, 2018.

[20] J. Lappalainen, "Calcium activity in astrocytes," B.S. thesis, 2018.

[21] M. De Pittà and H. Berry, "Computational glioscience," 2019.

[22] J. Lallouette, M. De Pittà, E. Ben-Jacob, and H. Berry, "Sparse short-distance connections enhance calcium wave propagation in a 3d model of astrocyte networks," *Frontiers in computational neuroscience*, vol. 8, p. 45, 2014.

[23] M. De Pittà, "Neuron-glial interactions," *arXiv preprint arXiv:2001.06881*, 2020.

[24] A. Araque, V. Parpura, R. P. Sanzgiri, and P. G. Haydon, "Tripartite synapses: glia, the unacknowledged partner," *Trends in neurosciences*, vol. 22, no. 5, pp. 208–215, 1999.

[25] S. Nadkarni and P. Jung, "Spontaneous oscillations of dressed neurons: a new mechanism for epilepsy?," *Physical review letters*, vol. 91, no. 26, p. 268101, 2003.

[26] I. Savtchouk and A. Volterra, "Gliotransmission: beyond black-and-white," *Journal of Neuroscience*, vol. 38, no. 1, pp. 14–25, 2018.

[27] T. A. Fiacco and K. D. McCarthy, "Multiple lines of evidence indicate that gliotransmission does not occur under physiological conditions," *Journal of Neuroscience*, vol. 38, no. 1, pp. 3–13, 2018.

[28] T. Papouin, L. Ladépêche, J. Ruel, S. Sacchi, M. Labasque, M. Hanini, L. Groc, L. Pollegioni, J.-P. Mothet, and S. H. Oliet, "Synaptic and extrasynaptic nmda receptors are gated by different endogenous coagonists," *Cell*, vol. 150, no. 3, pp. 633–646, 2012.

[29] S. Ramón y Cajal, "The croonian lecture.—la fine structure des centres nerveux," *Proceedings of the Royal Society of London*, vol. 55, no. 331-335, pp. 444–468, 1894.

[30] V. Castellucci, H. Pinsker, I. Kupfermann, and E. R. Kandel, "Neuronal mechanisms of habituation and dishabituation of the gill-withdrawal reflex in aplysia," *Science*, vol. 167, no. 3926, pp. 1745–1748, 1970.

[31] D. O. Hebb, "The organization of behavior: A neuropsychological theory," 2005.

[32] C. Constantinidis, S. Funahashi, D. Lee, J. D. Murray, X.-L. Qi, M. Wang, and A. F. Arnsten, "Persistent spiking activity underlies working memory," *Journal of neuroscience*, vol. 38, no. 32, pp. 7020–7028, 2018.

[33] M. Lundqvist, P. Herman, and E. K. Miller, "Working memory: delay activity, yes! persistent activity? maybe not," *Journal of neuroscience*, vol. 38, no. 32, pp. 7013–7019, 2018.

[34] M. G. Stokes, "'activity-silent'working memory in prefrontal cortex: a dynamic coding framework," *Trends in cognitive sciences*, vol. 19, no. 7, pp. 394–405, 2015.

[35] A. Compte, N. Brunel, P. S. Goldman-Rakic, and X.-J. Wang, "Synaptic mechanisms and network dynamics underlying spatial working memory in a cortical network model," *Cerebral cortex*, vol. 10, no. 9, pp. 910–923, 2000.

[36] Y. Loewenstein and H. Sompolinsky, "Temporal integration by calcium dynamics in a model neuron," *Nature neuroscience*, vol. 6, no. 9, pp. 961–967, 2003.

[37] G. Mongillo, O. Barak, and M. Tsodyks, "Synaptic theory of working memory," *Science*, vol. 319, no. 5869, pp. 1543–1546, 2008.

[38] M. De Pitta, V. Volman, H. Levine, and E. Ben-Jacob, "Multimodal encoding in a simplified model of intracellular calcium signaling," *Cognitive processing*, vol. 10, no. 1, p. 55, 2009.

[39] M. De Pittà and N. Brunel, "Multiple forms of working memory emerge from synapse-astrocyte interactions," *PNAS*, 2022.

[40] S. Becker, A. Nold, and T. Tchumatchenko, "Modulation of working memory duration by synaptic and astrocytic mechanisms," *PLoS Computational Biology*, vol. 18, no. 10, p. e1010543, 2022.

[41] E. M. Izhikevich, "Which model to use for cortical spiking neurons?," *IEEE transactions on neural networks*, vol. 15, no. 5, pp. 1063–1070, 2004.

[42] T. Manninen, R. Havela, and M.-L. Linne, "Computational models for calcium-mediated astrocyte functions," *Frontiers in computational neuroscience*, vol. 12, p. 14, 2018.

[43] L. Lapique, "Recherches quantitatives sur l'excitation electrique des nerfs traitee comme une polarization.," *Journal of Physiology and Pathololgy*, vol. 9, pp. 620–635, 1907.

[44] A. L. Hodgkin and A. F. Huxley, "A quantitative description of membrane current and its application to conduction and excitation in nerve," *The Journal of physiology*, vol. 117, no. 4, pp. 500–544, 1952.

[45] E. M. Izhikevich, "Simple model of spiking neurons," *IEEE Transactions on neural networks*, vol. 14, no. 6, pp. 1569–1572, 2003.

[46] S. Y. Gordleeva, S. V. Stasenko, A. V. Semyanov, A. E. Dityatev, and V. B. Kazantsev, "Bi-directional astrocytic regulation of neuronal activity within a network," *Frontiers in computational neuroscience*, vol. 6, p. 92, 2012.

[47] M. V. Tsodyks and H. Markram, "The neural code between neocortical pyramidal neurons depends on neurotransmitter release probability," *Proceedings of the national academy of sciences*, vol. 94, no. 2, pp. 719–723, 1997.

[48] Y.-X. Li and J. Rinzel, "Equations for insp3 receptor-mediated [ca2+] i oscillations derived from a detailed kinetic model: a hodgkin-huxley like formalism," *Journal of theoretical Biology*, vol. 166, no. 4, pp. 461–473, 1994.

[49] G. W. De Young and J. Keizer, "A single-pool inositol 1, 4, 5-trisphosphate-receptor-based model for agonist-stimulated oscillations in ca2+ concentration.," *Proceedings of the National Academy of Sciences*, vol. 89, no. 20, pp. 9895–9899, 1992.

[50] D. E. Postnov, R. Koreshkov, N. Brazhe, A. R. Brazhe, and O. V. Sosnovtseva, "Dynamical patterns of calcium signaling in a functional model of neuron–astrocyte networks," *Journal of biological physics*, vol. 35, no. 4, pp. 425–445, 2009.

[51] T. Höfer, L. Venance, and C. Giaume, "Control and plasticity of intercellular calcium waves in astrocytes: a modeling approach," *Journal of Neuroscience*, vol. 22, no. 12, pp. 4850–4859, 2002.

[52] M. De Pittà, M. Goldberg, V. Volman, H. Berry, and E. Ben-Jacob, "Glutamate regulation of calcium and ip 3 oscillating and pulsating dynamics in astrocytes," *Journal of biological physics*, vol. 35, no. 4, pp. 383–411, 2009.

[53] G. Ullah, P. Jung, and A. H. Cornell-Bell, "Anti-phase calcium oscillations in astrocytes via inositol (1, 4, 5)-trisphosphate regeneration," *Cell calcium*, vol. 39, no. 3, pp. 197–208, 2006.

[54] H. K. Khalil, *Nonlinear control*, vol. 406. Pearson New York, 2015.

[55] V. Würzbauer, K. Lenk, and M. Jafarian, "Astrocytic gliotransmission as a pathway for stable stimulation of post-synaptic spiking: Implications for working memory," *arXiv preprint arXiv:2304.06004*, 2023.

[56] P. De Leenheer and D. Aeyels, "Stability properties of equilibria of classes of cooperative systems," *IEEE Transactions on Automatic Control*, vol. 46, no. 12, pp. 1996–2001, 2001.

[57] N. Kopell and B. Ermentrout, "Chemical and electrical synapses perform complementary roles in the synchronization of interneuronal networks," *Proceedings of the National Academy of Sciences*, vol. 101, no. 43, pp. 15482–15487, 2004.

[58] Y. Tsybina, S. Gordleeva, M. Krivonosov, I. Kastalskiy, A. Zaikin, and A. Gorban, "Modelling working memory in neuron-astrocyte network," in *2021 International Joint Conference on Neural Networks (IJCNN)*, pp. 1–6, IEEE, 2021.

[59] Y. Tsybina, I. Kastalskiy, M. Krivonosov, A. Zaikin, V. Kazantsev, A. N. Gorban, and S. Gordleeva, "Astrocytes mediate analogous memory in a multi-layer neuron–astrocyte network," *Neural Computing and Applications*, vol. 34, no. 11, pp. 9147–9160, 2022.

[60] G. A. Miller, "The magical number seven, plus or minus two: Some limits on our capacity for processing information.," *Psychological review*, vol. 63, no. 2, p. 81, 1956.

[61] P. Allegrini, L. Fronzoni, and D. Pirino, "The influence of the astrocyte field on neuronal dynamics and synchronization," *Journal of biological physics*, vol. 35, no. 4, pp. 413–423, 2009.

[62] M. Amiri, N. Hosseinmardi, F. Bahrami, and M. Janahmadi, "Astrocyte-neuron interaction as a mechanism responsible for generation of neural synchrony: a study based on modeling and experiments," *Journal of computational neuroscience*, vol. 34, no. 3, pp. 489–504, 2013.

[63] S. Nazari, K. Faez, and M. Amiri, "A multiplier-less digital design of a bio-inspired stimulator to suppress synchronized regime in a large-scale, sparsely connected neural network," *Neural Computing and Applications*, vol. 28, no. 2, pp. 375–390, 2017.

[64] R. Brette, M. Rudolph, T. Carnevale, M. Hines, D. Beeman, J. M. Bower, M. Diesmann, A. Morrison, P. H. Goodman, F. C. Harris, *et al.*, "Simulation of networks of spiking neurons: a review of tools and strategies," *Journal of computational neuroscience*, vol. 23, no. 3, pp. 349–398, 2007.

[65] M. L. Hines and N. T. Carnevale, "The neuron simulation environment," *Neural computation*, vol. 9, no. 6, pp. 1179–1209, 1997.

[66] N. T. Carnevale and M. L. Hines, *The NEURON book*. Cambridge University Press, 2006.

[67] L. P. Savtchenko, L. Bard, T. P. Jensen, J. P. Reynolds, I. Kraev, N. Medvedev, M. G. Stewart, C. Henneberger, and D. A. Rusakov, "Disentangling astroglial physiology with a realistic cell model in silico," *Nature communications*, vol. 9, no. 1, pp. 1–15, 2018.

[68] J. C. Butcher, *Numerical methods for ordinary differential equations*. John Wiley & Sons, 2016.